Structural basis of potent Zika–dengue virus antibody cross-neutralization

Giovanna Barba-Spaeth, Wanwisa Dejnirattisai, Alexander Rouvinski, Marie-Christine Vaney, Iris Medits, Arvind Sharma, Etienne Simon-Lorière, Anavaj Sakuntabhai, Van-Mai Cao-Lormeau, Ahmed Haouz, et al.

Structural basis of Zika and Dengue virus potent antibody cross-neutralization

Giovanna Barba-Spaeth[1,2,#], Wanwisa Dejnirattisai[3,#], Alexander Rouvinski[1,2,#], Marie-Christine Vaney[1,2,#], Iris Medits[4], Arvind Sharma[1,2], Etienne Simon-Lorière[5,6], Anavaj Sakuntabhai[5,6], Van-Mai Cao-Lormeau[7], Ahmed Haouz[8], Patrick England[9], Karin Stiasny[4], Juthathip Mongkolsapaya[3,10], Franz X. Heinz[4*], Gavin R. Screaton[3*] and Félix A. Rey[1,2*]

[1]*Institut Pasteur, Unité de Virologie Structurale, Département de Virologie, F-75724 Paris Cedex 15, France.*
[2]*CNRS UMR 3569 Virologie, F-75724 Paris Cedex 15, France*
[3]*Division of Immunology and Inflammation, Department of Medicine, Hammersmith campus, Imperial College London, UK*
[4]*Department of Virology, Medical University of Vienna, Kinderspitalgasse 15, A-1095 Vienna, Austria*
[5]*Institut Pasteur, Unité de Génétique fonctionnelle des maladies infectieuses, Département de Génomes et Génétique, F-75724 Paris Cedex 15, France*
[6]*CNRS URA 3012, F-75724 Paris Cedex 15, France*
[7]*Unit of Emerging Infectious Diseases, Institut Louis Malardé, Papeete,Tahiti,French Polynesia*
[8]*Institut Pasteur, Plateforme de Cristallographie, Département de Biologie Structurale et Chimie, F-75724 Paris Cedex 15, France.*
[9]*Institut Pasteur, Plateforme de Biophysique des Macromolécules et de leurs Interactions, Département de Biologie Structurale et Chimie, F-75724 Paris Cedex 15, France.*
[10]*Dengue Hemorrhagic Fever Research Unit, Office for Research and Development, Siriraj Hospital, Faculty of Medicine, Mahidol University, Bangkok, Thailand.*
[#]*These authors contributed equally and are listed in alphabetical order.*

Correspondence: felix.rey@pasteur.fr (FAR); g.screaton@imperial.ac.uk (GRS);
Franz.X.Heinz@meduniwien.ac.at (FXH).

Zika virus is a member of the flavivirus genus that had not been associated with severe disease in humans until the recent outbreaks, when it was linked to microcephaly in newborns in Brazil and to Guillain-Barré Syndrome in adults in French Polynesia. Zika virus is related to dengue virus, and we report here that a category of antibodies isolated from dengue patients and targeting a conformational epitope potently neutralize Zika virus. The crystal structure of two of these antibodies in complex with the envelope protein of Zika virus reveals the details of a conserved epitope, which is also the site of interaction of the envelope protein dimer with the precursor prM protein during virus maturation. Comparison of the Zika and dengue virus immunocomplexes provides a lead for a rational, epitope-focused design of a universal vaccine capable of eliciting potent cross-neutralizing antibodies to protect against Zika and dengue viruses simultaneously.

Zika virus (ZIKV) is an arthropod-borne enveloped virus belonging to the flavivirus genus in the family *Flaviviridae*, which also includes the human pathogenic yellow fever, dengue, West Nile and tick-borne encephalitis viruses[1]. Flaviviruses have two structural glycoproteins, prM and E (for precursor Membrane and Envelope proteins, respectively), which form a heterodimer in the endoplasmic reticulum (ER) of the infected cell and drive the budding of spiky immature virions into the ER lumen. These particles transit through the cellular secretory pathway, during which the trans-Golgi protease, furin, cleaves prM. This processing, required for infectivity, results in loss of a large fragment of prM and reorganization of E on the virion surface. The mature particles have a smooth aspect, with 90 E dimers organized with icosahedral symmetry in a "herringbone" pattern[2,3].

Three-dimensional cryo-EM structures of the mature ZIKV particles have recently been reported to near atomic resolution (3.8 Å)[4,5], showing that it has essentially the same organization as the other flaviviruses of known structure, such as dengue virus (DENV) [3] and West Nile virus[6,7]. The E protein is about 500 amino acids long, with the 400 N-terminal residues forming the ectodomain essentially folded as β-sheets with three domains named I, II and III, aligned in a row with domain I at the center. The conserved fusion loop is at the distal end of the rod in domain II, buried at the E dimer interface. At the C-terminus, the E ectodomain is followed by the so-called "stem", featuring two α-helices lying flat on the viral membrane (the "stem" helices), which link to two C-terminal trans-membrane α-helices. The main distinguishing feature of the ZIKV virion is an insertion within a glycosylated loop of E (the "150" loop), which protrudes from the mature virion surface[4,5].

Flaviviruses have been grouped into serocomplexes based on cross-neutralization studies with polyclonal immune sera[8]. The E protein is the main target of neutralizing antibodies, and is also the viral fusogen; cleavage of prM allows E to respond to the endosomal pH by undergoing a large-scale conformational change that catalyzes membrane fusion and releases the viral genome into the cyotosol. Loss of the precursor fragment of prM lets the E protein fluctuate from its tight packing at the surface of the virion, transiently exposing otherwise buried surfaces. One surface exposed by this "breathing" is the fusion-loop epitope (FLE), which is a dominant cross-reactive antigenic site[9]. Although antibodies to this site can protect by complement-mediated mechanisms, as shown for West Nile virus in a mouse model[10], they are poorly neutralizing and lead to antibody-dependent enhancement (ADE)[11-15] thereby aggravating flavivirus pathogenesis and complicating the development of safe and effective vaccines.

We recently reported the isolation and structural characterization of a panel of antibodies isolated from dengue patients[13,16]. Most of these antibodies target the FLE, but others target a quaternary site readily accessible at the exposed surface of the E protein on the virion, at the interface between the two E subunits in the dimer. These broadly neutralizing antibodies (bnAbs), termed EDE for "E-dimer epitope", potently neutralize all four serotypes of DENV. Their binding site is conserved across serotypes because it is also the interaction site of prM with E dimers during transport of the immature virus particles through the Golgi apparatus of the cell. There were two subsets of EDE Mabs, characterized by a differential requirement for glycosylation on the 150 loop for binding. The EDE1 bnAbs bind better in the absence of glycan, whereas EDE2 bnAbs bind better when the glycan is present.

In this study we show that the EDE Mabs neutralize ZIKV as potently as they neutralize DENV. We also find that the FLE antibodies, which neutralize DENV - although not as potently as the EDE Mabs - do not neutralize ZIKV at concentrations up to 1μM in spite of a high affinity for the recombinant ZIKV E protein. We further describe the crystal structures of the ZIKV E protein dimer alone and in complex with EDE1 C8 and EDE2 A11, identifying their binding determinants.

A ZIKV-DENV super serogroup

Phylogenetic analyses of the main human pathogenic flaviviruses using the amino acid sequences of the viral RNA polymerase NS5 indicate a clustering of ZIKV with the group of mosquito-borne encephalitic viruses (Fig. 1a). The clustering is different when the amino acid sequences of the E protein are considered, with ZIKV branching with the DENV group. If the sequence clustering extends to the antigenic surface of E, antibodies that cross-react with several DENV serotypes should also bind ZIKV E. To test this hypothesis we used bio-layer interferometry (BLI) to study the binding properties of a poorly neutralizing, cross-reactive FLE antibody and the potently neutralizing EDE mAbs for recombinant, soluble ZIKV E ectodomain (ZIKV sE) produced in insect cells (see Online methods). The FLE mAb (P6B10) bound nearly 10fold more tightly than did EDE1 C8 (apparent Kd ~1.5 nM vs. 9 nM) and nearly 1000 times more tightly than EDE2 A11 (Fig. 1b and ED Fig. 1a). Consistent with their affinities, we could isolate a complex of ZIKV sE with a C8 Fab by SEC, but not with an A11 Fab (ED Fig. 1b).

Neutralization assays in African green monkey (VERO) cells using these and other members of the three antibody subsets, showed that the EDE1 antibodies strongly neutralize ZIKV, whereas the EDE2 were at least one log less potent. In spite of its strong affinity, P6B10 did not neutralize in the concentration range used, nor did any of the two other FLE antibodies tested (Fig. 2). The EDE1 bnAbs neutralized better the African strain HD78788, which has over the years been cell-culture adapted and

passaged in suckling mice brain, and lacks E glycosylation. The IC50 against the PF13 strain, isolated in French Polynesia in 2013 and in which the E protein is glycosylated at position 154, was in the nanomolar range and comparable to - or lower than – that against the four serotypes of DENV (Table 1). The EDE2 bnAbs showed no difference in neutralization of the two strains, suggesting that the presence of the N154 glycan in the ZIKV E protein did not enhance the interaction.

The ZIKV / EDE bnAbs immune complexes

We crystallized unliganded ZIKV sE and complexes of ZIKV sE with EDE1 C8 and EDE2 A11 with scFv and Fab fragments, respectively (ED Table1). In the structure of unliganded ZIKV sE, the 150 loop is ordered, unlike the unglycosylated 150 loop in the recently determined structure of the protein produced in bacteria and refolded in vitro[17]. In contrast to our insect-cell secreted protein, which is a dimer (ED Fig. 1b) the refolded protein was reported to be monomeric in solution, suggesting that the glycan may help structure the loop and promote sE dimerization.

The antibodies recognize a quaternary epitope in the ZIKV sE dimer in the same way they recognize the DENV serotype 2 (DENV-2) sE dimer described earlier[16]. The amino-acid residues participating in the contacts, for both the ZIKV and DENV-2 structures, are shown in ED Fig. 2. The pattern is, as expected, very similar, with the few differences highlighted in red frames in ED Fig. 2b. Both epitopes in the sE dimer are occupied in the case of the complex with C8 (Fig. 3a) whereas only one is occupied in the case of A11 (Fig. 4a). Inspection of the crystal environment showed that a second Fab could not be docked at this position without clashing with neighboring complexes in the crystal. This observation indicates that crystal growth selected for incorporation of sE dimers with a single Fab bound, which is facilitated by the low affinity of A11.

The bnAbs dock on ZIKV sE at different angles than they do on DENV-2 sE (see insets in Figs. 3a and 4a). In the case of the C8 complex, the difference in docking results mainly from an altered curvature of the sE dimer. We note that the conformation of ZIKV sE in complex with the antibodies is very similar to the one it adopts on the virus particle, with roughly 1.5 Å root mean square deviation (RMSD) for 790 Cα atoms (see ED Table 2). The unbound ZIKV sE crystallized here displays a more distant conformation (2.5 Å RMSD when comparing to both virion ZIKV E and either of the sE antibody complexes), suggesting that the antibodies stabilize a conformation close to that on the viral particle. In contrast, the same comparisons done for DENV-2 sE, alone or in complex with the bnAbs result in RMSD values of 5-7 Å with respect to the E conformation on the DENV virion observed by cryo-EM[3]. For comparison, superposition of the ectodomain of virion E from ZIKV[5] and DENV-2 [3] results in a similar 1.5 Å RMSD, indicating that they are presented roughly in the same way, but that DENV sE is more deformable in solution.

This malleability may reflect the conformational breathing reported for DENV E[18]. Instead, ZIKV sE remains in a similar conformation in the absence of the interactions with the underlying stem α-helices and with the M protein (the membrane-anchored remnant of prM after furin cleavage) on the virion, in line with the higher stability of the ZIKV particles described recently[4].

EDE1 C8 complex

The total buried surface area of EDE1 in the complex with ZIKV sE is about 900 Å^2, compared to about 1300 Å^2 in the DENV-2 sE complex (ED Table 3). Fig. 3d shows the conservation of the epitope, and Figs. 3e and 3f compare the C8 footprint on ZIKV and DENV-2 sE. The DENV-specific glycan at position N67, which is ordered in the DENV-2 sE structure (Fig. 3c), accounts for around two-thirds of the overall difference in footprint area. The N67 glycan interacts with the framework region 2 of the heavy chain (FRH2), and its absence in ZIKV sE shows that these contacts are not essential for binding. The key cluster of interactions that is maintained is centered on β-strand *b* of domain II, with side chains from CDRs H2, H3 and L3 recognizing all the available hydrogen bond donors (NH atoms) and acceptors (main chain carbonyls) of the *bdc* β-sheet edge (Figs. 3b and 3c). In addition, the fusion loop main chain (which contains several glycine residues) and the disulfide bond between Cys74 and Cys105, are framed by aromatic side chains of the CDRs L1 and L3 (see also ED Figure 3). Residues from these two CDRs also recognize strictly conserved side chains of the fusion loop (Arg 99) or nearby (Gln 77).

Across the dimer interface, and as in the complex with DENV-2, the 150 loop is partially disordered, with no detectable density for the N154 glycan (Fig. 3a and ED Fig. 3d). As shown in ED Fig. 3, the interacting residues across the dimer interface are different, reflecting the more limited sequence conservation in these regions of the E protein: in the DENV-2 sE complex, these contacts are with β-strands A and B of domain III, but in ZIKV they mainly involve Lys 373 from β-strand E interacting with CDRs L1 and L2, with a network of direct or water-mediated hydrogen bonds (ED Figs. 3b and 3c). Similarly, a number of charged residues in domain I and from the nearby *kl* loop of domain II across the interface, contribute to the binding and interact with the heavy chain CDRs H2 and H3 (ED Figs. 3e and 3f). All the polar interactions between C8 and ZIKV sE are listed in ED Tables 4 and 5, and the electrostatic surface of the epitope is displayed in ED Fig. 4, left panel. In summary, these observations identify the conserved cluster of contacts with the *b* strand and the fusion loop in domain II as the main binding determinants of C8, with additional contacts from across the dimer interface - or from the N67 glycan in DENV - further stabilizing but not determining the interaction.

EDE2 A11 complex

ED Figure 4 compares the footprint of C8 and A11 on ZIKV sE, together with the surface electrostatic potential of the complexes, which shows a strong basic patch on sE in the C8 complex due to the disorder of the 150 loop. As shown in ED Fig. 5, C8 would clash with the glycan had the loop remained in place, as was the case in the complex with DENV-2 sE[16]. In the A11 complex the 150 loop remains in the same conformation as in the cryo-EM structures of the virion (ED Fig. 5a) and in the X-ray structure of glycosylated unliganded sE reported here. In the DENV-2 sE / A11 complex, the glycan is recognized by an α-helix in the long CDR3 loop (Fig. 4e). The difference in length in the 150 loop of E in ZIKV compared to DENV shifts the glycan position by about 6-7Å, such that it cannot make the same interactions with the CDR H3 α-helix (Figs. 4d and e and ED Fig. 5b). As a consequence, the A11 antibody docks at a different angle on ZIKV sE than it does on DENV-2 sE, even accounting for the difference in sE dimer curvature (Fig. 4a, inset). The contacts along the *b*-strand are preserved (Fig. 4b and c). Compared to C8, the *b* strand is recognized only at its end (residues 71 and 73), whereas C8 recognizes it all along, from residue 68 (or from 67 in DENV).

DISCUSSION

Our results identify the structural details of a quaternary epitope that provides a previously unrecognized link of potent cross-neutralization between Zika and dengue viruses, and thus identifies an antigenic flavivirus cluster beyond the traditional serocomplexes. This relationship defines a super serogroup on the basis of strong cross-neutralization through a conserved epitope that had not been recognized using polyclonal sera[8]. This finding thus introduces the possibility of developing a universal vaccine protecting against all the viruses from this group.

Vaccine design against dengue virus has been hampered by the heterogeneity of DENV particles and the need to use polyvalent formulas to immunize against all four serotypes [19,20]. One feature of DENV is that it undergoes incomplete furin maturation cleavage of prM in many cell types, giving rise to heterogeneous mosaic particles with an immature-like spiky patch on one side and a smooth mature-like region on the opposite side[21]. These particles are infectious, as they can fuse with the cellular membrane through the smooth, mature side. Because the FLE is exposed in immature regions[22], most of the antibody response in DENV infected patients is directed against it [23]. These cross-reactive antibodies coat the particles on the "immature side"[22] but neutralize only weakly, because they can bind the "mature side" only when the E protein "breathes"[24-26]. A recently published structure of monomeric ZIKV sE in complex with an FLE-specific monoclonal murine antibody of low neutralizing activity indeed shows that its binding site would be occluded in the dimeric E protein on mature infectious virions[17].

The observation that P6B10 and other FLE antibodies still neutralize DENV[13] suggests that E in the mature patches on DENV spends more time in conformations that expose the FLE than does E in those patches on ZIKV. This inference is consistent with the high thermal stability of ZIKV reported recently[4].

Our results suggest that the epitope targeted by the EDE1 bnAbs is better suited for developing an epitope-focused vaccine for viruses in the ZIKV/DENV super-serogroup than is the FLE, which induces poorly neutralizing and strongly infection-enhancing antibodies[12-14]. The EDE1 is also better suited than the related EDE2 epitope: although the EDE1 Mabs require an E dimer to bind, the actual binding determinants are centered on the *b* strand and on the highly conserved, E-dimer-exposed elements of the fusion loop, as shown by the comparison between their binding to DENV-2 and ZIKV sE. The fact that EDE2 bnAbs rely heavily in their contact points on the adjacent subunit - on the variable 150 loop in which glycosylation is not always present - is a drawback, as demonstrated by their poor affinity (Fig. 1) and by their strong induction of ADE[12].

Targeting the *b* strand and the E-dimer exposed elements of the fusion loop appears as a powerful alternative to the multi-immunogen approaches against the DENV cluster that have had limited success in clinical trials[27]. As the E protein polypeptide chain displays neither insertions nor deletions in the region of the *b* strand for any medically relevant flavivirus, this region presents a low risk of inducing escape mutations, most likely because it is also the interacting site with prM during virus maturation. Finally, in a more immediate application, our study also suggests that the EDE1 antibodies – perhaps carrying the "LALA" mutation [28] if effector functions are to be avoided - could be useful for immune prophylaxis for pregnant women at risk of contracting ZIKV infection.

References

1 Lindenbach, B., Murray, C., Thiel, H. & Rice, C. *Flaviviridae: the viruses and their replication*. 6th edn, Vol. 1 1101-1152 (Lippincott Williams & Wilkins, 2013).

2 Kuhn, R. J. *et al.* Structure of dengue virus: implications for flavivirus organization, maturation, and fusion. *Cell* **108**, 717-725 (2002).

3 Zhang, X. *et al.* Cryo-EM structure of the mature dengue virus at 3.5-A resolution. *Nat Struct Mol Biol* **20**, 105-110, doi:10.1038/nsmb.2463 (2013).

4 Kostyuchenko, V. A. *et al.* Structure of the thermally stable Zika virus. *Nature*, doi:10.1038/nature17994 (2016).

5 Sirohi, D. *et al.* The 3.8 A resolution cryo-EM structure of Zika virus. *Science* **352**, 467-470, doi:10.1126/science.aaf5316 (2016).

6 Mukhopadhyay, S., Kim, B. S., Chipman, P. R., Rossmann, M. G. & Kuhn, R. J. Structure of West Nile virus. *Science* **302**, 248, doi:10.1126/science.1089316 (2003).

7 Zhang, W., Kaufmann, B., Chipman, P. R., Kuhn, R. J. & Rossmann, M. G. Membrane curvature in flaviviruses. *J Struct Biol* **183**, 86-94, doi:10.1016/j.jsb.2013.04.005 (2013).

8 Calisher, C. H. *et al.* Antigenic relationships between flaviviruses as determined by cross-neutralization tests with polyclonal antisera. *The Journal of general virology* **70 (Pt 1)**, 37-43, doi:10.1099/0022-1317-70-1-37 (1989).

9 Stiasny, K., Kiermayr, S., Holzmann, H. & Heinz, F. X. Cryptic properties of a cluster of dominant flavivirus cross-reactive antigenic sites. *J Virol* **80**, 9557-9568, doi:10.1128/JVI.00080-06 (2006).

10 Vogt, M. R. *et al.* Poorly neutralizing cross-reactive antibodies against the fusion loop of West Nile virus envelope protein protect in vivo via Fcgamma receptor and complement-dependent effector mechanisms. *J Virol* **85**, 11567-11580, doi:10.1128/JVI.05859-11 (2011).

11 Balsitis, S. J. *et al.* Lethal antibody enhancement of dengue disease in mice is prevented by Fc modification. *PLoS Pathog* **6**, e1000790, doi:10.1371/journal.ppat.1000790 (2010).

12 Dejnirattisai, W. *et al.* Dengue serocrossreactivity drives antibody dependent enhancement of Zika virus infection. *(Sumitted, related manuscript)* (2016).

13 Dejnirattisai, W. *et al.* A new class of highly potent, broadly neutralizing antibodies isolated from viremic patients infected with dengue virus. *Nat Immunol* **16**, 170-177, doi:10.1038/ni.3058 (2015).

14 Goncalvez, A. P., Engle, R. E., St Claire, M., Purcell, R. H. & Lai, C. J. Monoclonal antibody-mediated enhancement of dengue virus infection in vitro and in vivo and strategies for prevention. *Proceedings of the National Academy of Sciences of the United States of America* **104**, 9422-9427, doi:10.1073/pnas.0703498104 (2007).

15 Halstead, S. B. In vivo enhancement of dengue virus infection in rhesus monkeys by passively transferred antibody. *J Infect Dis* **140**, 527-533 (1979).

16 Rouvinski, A. *et al.* Recognition determinants of broadly neutralizing human antibodies against dengue viruses. *Nature* **520**, 109-113, doi:10.1038/nature14130 (2015).

17 Dai, L. *et al.* Structures of the Zika Virus Envelope Protein and Its Complex with a Flavivirus Broadly Protective Antibody. *Cell Host Microbe*, doi:10.1016/j.chom.2016.04.013 (2016).

18 Kuhn, R. J., Dowd, K. A., Beth Post, C. & Pierson, T. C. Shake, rattle, and roll: Impact of the dynamics of flavivirus particles on their interactions with the host. *Virology* **479-480**, 508-517, doi:10.1016/j.virol.2015.03.025 (2015).

19 Sabchareon, A., Wallace, D., Lang, J., Bouckenooghe, A. & Moureau, A. Efficacy of tetravalent dengue vaccine in Thai schoolchildren - Authors' reply. *Lancet* **381**, 1094-1095, doi:10.1016/S0140-6736(13)60755-2 (2013).

20 Vannice, K. S., Durbin, A. & Hombach, J. Status of vaccine research and development of vaccines for dengue. *Vaccine*, doi:10.1016/j.vaccine.2015.12.073 (2016).

21 Plevka, P. *et al.* Maturation of flaviviruses starts from one or more icosahedrally independent nucleation centres. *EMBO Rep* **12**, 602-606, doi:10.1038/embor.2011.75 (2011).
22 Cherrier, M. V. *et al.* Structural basis for the preferential recognition of immature flaviviruses by a fusion-loop antibody. *EMBO J* **28**, 3269-3276, doi:10.1038/emboj.2009.245 (2009).
23 Beltramello, M. *et al.* The human immune response to Dengue virus is dominated by highly cross-reactive antibodies endowed with neutralizing and enhancing activity. *Cell Host Microbe* **8**, 271-283, doi:10.1016/j.chom.2010.08.007 (2010).
24 Dowd, K. A., Mukherjee, S., Kuhn, R. J. & Pierson, T. C. Combined effects of the structural heterogeneity and dynamics of flaviviruses on antibody recognition. *J Virol* **88**, 11726-11737, doi:10.1128/JVI.01140-14 (2014).
25 Lee, P. D. *et al.* The Fc region of an antibody impacts the neutralization of West Nile viruses in different maturation states. *J Virol* **87**, 13729-13740, doi:10.1128/JVI.02340-13 (2013).
26 Mukherjee, S. *et al.* Mechanism and significance of cell type-dependent neutralization of flaviviruses. *J Virol* **88**, 7210-7220, doi:10.1128/JVI.03690-13 (2014).
27 Capeding, M. R. *et al.* Clinical efficacy and safety of a novel tetravalent dengue vaccine in healthy children in Asia: a phase 3, randomised, observer-masked, placebo-controlled trial. *Lancet* **384**, 1358-1365, doi:10.1016/S0140-6736(14)61060-6 (2014).
28 Hessell, A. J. *et al.* Fc receptor but not complement binding is important in antibody protection against HIV. *Nature* **449**, 101-104, doi:10.1038/nature06106 (2007).

Acknowledgements. We thank the Maria van Kerkhove, the 'working group ZIKA' and our colleagues in the Unité de Virologie Structurale at Institut Pasteur for help and discussions; the staff at the crystallogenesis platform and the recombinant proteins platform of the Institut Pasteur; Patricia Sylvestre and the Risk Prevention Unit of the Institut Pasteur for their biosafety expertise; William Shepard and Pierre Legrand for help during data collection and for discussions; the staff at beamlines PX1 and PX2 at SOLEIL synchrotron (Saclay, France), the staff at beamline ID23-2 at the European Synchrotron Radiation Facility (Grenoble, France) and staff at beamline PX1 at the Swiss Light Source synchrotron (Villigen, Switzerland); Gérard Bricogne for suggestions on processing anisotropic diffraction data; Andrea Reiter and Hannes Prechler for help in recombinant sE production. FAR and AS acknowledge support from the European Commission FP7 Programme for the DENFREE project under Grant Agreement n°282 378FP7. FAR also received funding from the "Integrative Biology of Emerging Infectious Diseases" Labex (Laboratoire d'Excellence) grant N° ANR-10-LABX-62-IBEID (French Government's “Investissements d'Avenir” program). FAR and KS also acknowledge the transnational ANR/FWF grant FlaviStem/I1378.

Author contributions: GBS did the first neutralization experiments and contributed throughout the project. VMCL, AS and ESL provided ZIKV from both strains, PF13 and HD78788. IM, KS and FXH provided the recombinant sE protein. AR and AS prepared recombinant antibody fragments; AR, GBS and WD did neutralization and binding experiments; AR grew the crystals and collected synchrotron data together with AH; MCV collected synchrotron data, processed the data, built, refined and analyzed the atomic models. ESL did the phylogenetic analyses; AR, AS and PE did the BLI experiments with recombinant sE. AR, GBS, KS, JM, FXH, GRS and FAR planned the experiments. FAR wrote the paper.

Author Information. Coordinates and structure factors amplitudes have been deposited in the Protein Data Bank under accession numbers XXX1, XXX2 and XXX3 for ZIKV sE/EDE1 C8 scFv, ZIKV sE/EDE2 A11 Fab complexes and ZIKV sE, respectively.

Competing financial interests. The EDE antibodies and epitope are the subject of a patent application by Imperial College and Institut Pasteur on which G.S., J.M., F.R., A.R., M.C.V. and G.B.S. are named as inventors.

FIGURE LEGENDS:

Figure 1: ZIKV/DENV E protein phylogeny and reactivity with DENV-elicited antibodies. **a)** Phylogenetic trees of the main human pathogenic flaviviruses based on the amino acid sequences of the E protein (left panel) and of the polymerase NS5 protein (right panel). The arthropod vectors are differentiated by the background color. **b)** ZIKV sE reactivity with human recombinant IgG mAbs FLE P6B10, EDE1 C8 and EDE2 A11. Left panel**:** Binding properties were monitored by Biolayer interferometry on Octet RED (ForteBio). The normalized response values expressed as fraction of binding site occupancy are plotted against concentrations of ZIKV sE dimer shown at logarithmic scale. Lines denote global curve fits used for Kd evaluation (see ED Fig. 1a for linear concentration range showing concentration dependent saturation fits). Normalized response values were deduced from individual sensograms of binding monitored at different ZIKV sE concentration (see right panel for EDE1 C8).

Figure 2: Neutralization curves using three antibodies each from the three subsets FLE, EDE1 and EDE2. The results represent the mean of four independent experiments done each in triplicate for PF13 and duplicate for HD78788 strains. The two ZIKV strains are in bright colors, red and blue. The neutralization data for the 4 DENV serotypes (dotted lines in pale colors) were taken from ref. [13], and are given here for comparison. The corresponding IC50 values are provided in Table 1. Note that the DENV4 strain used was a natural isolate lacking the N153 glycosylation site.

Figure 3: EDE1 C8 / ZIKV sE complex. **a)** Overall view of the complex, with the sE moiety colored by domains (I, II and III in red, yellow and blue, respectively, and the fusion loop in orange); the antibodies in grey and dark green for light and heavy chains, respectively. The CDRs are colored (H1 light blue, H2 sand, H3 pink, L1 light gray, L2 red, L3 orange). The inset shows a comparison with the corresponding DENV-2 complex. For clarity, the variable region of the C8 Fab fragment of the DENV-2 sE/C8 complex was superposed on the scFv in complex with ZIKV sE in order to draw the Fab axis and better show the docking angles. **b)** Zoom of the ZIKV sE/C8 interaction to show the recognition of the *b* strand. Hydrogen bonds are shown as dotted lines and immobilized water molecules as red spheres. **c)** Same region on the DENV-2 sE/C8 Fab complex. Note that the N67 glycan on DENV also interacts with the antibody. **d)** The footprint of EDE1 C8 is outlined on ZIKV sE dimer shown in surface representation (looking from outside the virion) colored according to conservation of surface exposed amino acids. Atoms from the main chain and conserved side chains are orange, highly similar side chains are yellow and all the others are white. **e, f)** Footprints of EDE1 C8 on a surface representation of ZIKV sE **(e)** and DENV-2 sE **(f)** shown in pink. The two protomers of sE in the dimer are in light and dark gray. Relevant antigenic sE regions

are labeled. Note the more confined interacting surface in ZIKV sE dimer than DENV-2, eg. N67 glycan is absent in ZIKV sE.

Figure 4: EDE2 A11 / ZIKV sE complex. Color coding is as in Fig. 3**. a)** Overall view of the complex, with only one Fab bound per sE dimer, due to crystal packing. The dashed ellipse represents the position of the missing A11 Fab. The inset compares the angle of binding to the sE dimer in ZIKV and in DENV-2. **b,c)** Interactions at the *b* strand in ZIKV (left panel) and in DENV-2 (right panel). Note the different angle of the *b* strand with respect to the antibody (the antibody is exactly in the same orientation in both panels) **d,e)** Zoom of the glycan on the 150 loop for ZIKV sE (d) and for DENV-2 sE (e), with sugar residue numbers described in the key. The CDR H3 helix is too far to make interactions with the glycan, as is the case in the DENV-2 structure (see ED Figs 2b and 5b).

METHODS

Recombinant production of ZIKV sE protein. Recombinant Zika virus sE protein (strain H/PF/2013, GenBank accession no. KJ776791) was produced with a tandem strep-tag in the Drosophila Expression System (Invitrogen) as described previously[29,30]. A chemically synthesized DNA fragment (GeneArt) containing the Zika sE sequence (amino acid 1-408) was cloned into the expression vector pT389 [31] that encodes the export signal sequence BIP, an enterokinase cleavage site and the strep-tag. Drosophila Schneider 2 cells were stably transfected using blasticidin for selection. Protein expression was induced by the addition of $CuSO_4$ and supernatants were harvested 7-10 days after induction. Antigens were purified via affinity chromatography with Streptactin columns (IBA) according to the manufacturer's instructions. A final purification gel filtration step used a Superdex increase 200 10/300 GL column equilibrated in 50 mM Tris pH8, 500 mM NaCl.

Production of antigen-binding (Fab) and single-chain Fv (scFv) fragments of the bnAbs. The bnAb fragments were cloned into plasmids for expression as Fab[32] and scFv[33] in Drosophila S2 cells. The constructs contain a tandem strep tag fused at the C-terminus (only of the heavy chain in the case of the Fab) for affinity purification. The purification protocol included a Streptactin affinity column followed by gel filtration as described above.

Expression of human monoclonal anti-DENV E antibodies. Full IgG antibodies were produced in 293T cells after co-transfection of plasmids containing heavy and light chains of immunoglobulin G1 as described in ref. [13].

Immune complex formation and isolation. The purified ZIKV sE protein was mixed with Fab A11 or scFv C8 (in approximately twofold molar excess) in standard buffer (500 mM NaCl, Tris 50 mM pH 8.0). The volume was brought to 0.5 ml by centrifugation in a Vivaspin 10 kDa cutoff; after 30 min incubation at 4°C, the complex was separated from excess Fab or scFv by size-exclusion chromatography (SEC) for ZIKV sE and scFv C8. For ZIKV sE and Fab A11 no apparent complex formation could be seen in SEC; therefore a solution containing sE at a concentration of 1.5 mg/ml and Fab A11 at a concentration of 3 mg/ml (corresponding to a molar ratio ~ 1:2 antigen:antibody) was directly used for crystallization. In all cases, the buffer was exchanged to 150 mM NaCl, 15 mM Tris, pH 8 for crystallization trials. The protein concentrations used for crystallization, determined by measuring the absorbance at 280 nm and using an extinction coefficient estimated from the amino-acid sequences, are listed in Extended Data Table 1.

Real-time biolayer interferometry binding assays. The interactions of purified ZIKV E protein with Mabs IgG FLE P6B10, IgG EDE1 C8, IgG EDE2 A11, and control Mabs IgG 28C (an anti-Influenza virus) were monitored in real-time using a Bio-layer interferometry Octet-Red384 device (Pall ForteBio). Anti-human IgG Fc capture biosensors (Pall ForteBio) were loaded for 10min at 1000 rpm shaking speed using antibodies at 5µg/ml in assay buffer (PBS+0.2 mg/ml BSA + tween 0.01%). Unbound antibodies were washed away for 1 min in assay buffer. IgG-loaded sensors were then incubated for 15 min at 1200 rpm in the absence and presence of two fold serially diluted ZIKV sE protein concentrations in assay buffer. Molar concentrations were calculated for the sE protein in a dimeric form. For Mabs FLE P6B10, EDE1 C8 and EDE2 A11, the following ZIKV sE concentration ranges : 50 - 0.78 nM, 200 - 3.125 nM and 3200 - 50 nM, were respectively used. Reference binding experiments were carried out in parallel on sensors loaded with control IgGs 28C. Dissociation of the complexes formed was then monitored for 10 min by dipping sensors in assay buffer alone. Operating temperature was maintained at 25 °C. The real-time data was analyzed using Scrubber 2.0 (Biologic Software) and Biaevaluation 4.1 (GE Healthcare). Specific signals were obtained by double-referencing, ie subtracting non-specific signals measured on non-specific IgG-loaded sensors and buffer signals on specific IgG-loaded sensors. Association and dissociation profiles, as well as steady-state signal vs concentration curves, were fitted assuming a 1 :1 binding model.

Crystallization and X-ray structure determinations. The crystallization and cryo-cooling conditions for diffraction data collection are listed in Extended Data Table 1. Crystallization trials were performed in sitting drops of 400 nl. Drops were formed by mixing equal volumes of the protein and reservoir solution in 96 wells Greiner plates, using a Mosquito robot and monitored by a Rock-Imager. Crystals were optimized using

a robotized Matrix Maker and Mosquito setups on 400 nl sitting or hanging drops, or manually in 24-well plates using 2–3 µl hanging drops.

Because of the strong anisotropy of the crystals (see results for anisotropy in Extended Data Table 1), an important number of crystals was tested at several beam lines at different synchrotrons (SOLEIL, St Aubin, France; ESRF, Grenoble, France; SLS, Villigen, Switzerland). The crystals having the less anisotropic diffraction data were used to solve the structures. The datasets were indexed, integrated, scaled and merged using XDS[34] and AIMLESS[35]. A preliminary model of ZIKV sE protein was built from the DENV-2 sE (4UTA) structure using the structure homology-modeling server SWISS-MODEL[36]. The structures of the complexes were then determined by molecular replacement with PHASER[37] using the search models listed in Extended Data Table 1. AIMLESS and PHASER programs were used within the CCP4 suite[38].

The DEBYE and STARANISO programs developed by Global Phasing Ltd. were applied to the AIMLESS scaled data without truncation of the resolution, using the STARANISO server (http://staraniso.globalphasing.org/). These softwares perform an anisotropic cut-off of merged intensity data with a Bayesian estimation of the structure amplitudes, and apply an anisotropic correction to the data. These corrected anisotropic amplitudes were then used for further refinement of both structures with BUSTER/TNT[39]. Please note that the Extended Data Table 1 shows the refinement statistics for the full sets of reflections truncated at the best high-resolution along h, k or l axis, values given by AIMLESS before the anisotropic corrections computed by STARANISO software.

The models were then alternatively manually corrected and completed using COOT[40] and refined using BUSTER/TNT against the amplitudes corrected for anisotropy. Refinements were constrained using non-crystallographic symmetry. The refined structures ZIKV sE / EDE1 C8 scFv, ZIKV sE / EDE2 A11 Fab and ZIKV sE have a final Rwork/Rfree (in %) of 19.2/22.1 and of 21.8/23.8 and of 20.8/23.6, respectively (see Extended Data Table 1).

Analysis of the atomic models and illustrations. Each complex was analyzed with the CCP4 suite of programs and the polar contacts were computed with the PISA website[41]. For the intermolecular interactions shown in Extended Data Figures 2 and 3 and Extended Data Tables 4 and 5, the maximal cutoff distances used were 4Å and 4.75Å for polar and van der Waals contacts, respectively. Multiple sequence alignments were calculated using Clustal W and Clustal X version 2 [42] on the EBI server[43]. All protein structure figures were prepared using ESPript[44] and the PyMOL Molecular Graphics System, version 1.5.0.4 (Schrödinger) (pymol. sourceforge.net).

Phylogenic trees. The Maximum likelihood phylogenetic trees were inferred using 12

representative amino-acid sequences of flaviviruses envelope protein E or RNA-polymerase NS5 proteins, utilizing the LG model available in PhyML[45] and a combination of SPR+NNI branch-swapping. Bootstrap values were calculated from 100 bootstrap replicates. The trees were visualized using Figtree (http://tree.bio.ed.ac.uk/software/figtree/). The accession codes of sequences used in the tree : Zika virus (ZIKV, KJ776791, strain H-PF-2013_French_Polynesia); dengue virus serotype 1 (DENV-1, NC_001477); dengue virus serotype 2 (DENV-2, NC_001474); dengue virus serotype 3 (DENV-3, NC_001475); dengue virus serotype 4 (DENV-4, NC_002640); Saint Louis encephalitis virus (SLEV, NC_007580); Japanese encephalitis virus (JEV, NC_001437; Murray Valley encephalitis *virus* (MVEV, NC_000943); West Nile virus (WNV, NC_001563); yellow fever virus (YFV, NC_002031); tick-borne encephalitis virus (TBEV, NC_001672); Powassan virus (POWV, NC_003687).

Viral stocks. The African strain Zika HD78788 was obtained from the Institut Pasteur collection and the Asian strain Zika PF13, isolated from a patient during ZIKV outbreak in French Polynesia in 2013, was obtained through the DENFREE (FP7/2007-2013) consortium. Viral stocks were prepared from supernatant of infected C6/36 cells (ATCC CRL-1660) clarified by centrifugation at 3000 g at 4°C and titrated on Vero cells (ATCC CRL-1586) by a focus-forming assay. Stocks were kept at -80°C until use. All cell lines were free from mycoplasma contamination.

Neutralization Assays. Virus neutralization by the tested human antibodies was evaluated using a focus reduction neutralization test (FRNT). About 100 ffu (focus forming unit) from virus stocks were incubated with a serial dilution of antibody for 1h at 37°C. The mixture was then added to Vero cells and foci were let to develop in presence of 1.5% methylcellulose for two days. Foci were then stained after fixation with 4% formaldehyde using anti-E 4G2 antibody (ATCC HB-112) and anti-mouse HRP-conjugated secondary antibody (ThermoFisher 31430). The foci were visualized by diaminobenzidine (DAB) (Sigma D5905) staining and plates were counted using the ImmunoSpot S6 Analyser (Cellular Technology Limited, CTL). Neutralization curves and 50% FRNT were calculated by non-linear regression analysis using Prism 6 software, GraphPad software.

METHODS REFERENCES

29 Vratskikh, O. *et al.* Dissection of antibody specificities induced by yellow fever vaccination. *PLoS Pathog* **9**, e1003458, doi:10.1371/journal.ppat.1003458 (2013).

30 Jarmer, J. *et al.* Variation of the specificity of the human antibody responses after tick-borne encephalitis virus infection and vaccination. *J Virol* **88**, 13845-13857, doi:10.1128/JVI.02086-14 (2014).

31 DuBois, R. M. *et al.* Functional and evolutionary insight from the crystal structure of rubella virus protein E1. *Nature* **493**, 552-556, doi:10.1038/nature11741 (2013).

32 Backovic, M. *et al.* Efficient method for production of high yields of Fab fragments in Drosophila S2 cells. *Protein Eng Des Sel* **23**, 169-174, doi:10.1093/protein/gzp088 (2010).

33 Gilmartin, A. A. *et al.* High-level secretion of recombinant monomeric murine and human single-chain Fv antibodies from Drosophila S2 cells. *Protein Eng Des Sel* **25**, 59-66, doi:10.1093/protein/gzr058 (2012).

34 Kabsch, W. Xds. *Acta crystallographica. Section D, Biological crystallography* **66**, 125-132, doi:10.1107/S0907444909047337 (2010).

35 Evans, P. R. & Murshudov, G. N. How good are my data and what is the resolution? *Acta crystallographica. Section D, Biological crystallography* **69**, 1204-1214, doi:10.1107/S0907444913000061 (2013).

36 Biasini, M. *et al.* SWISS-MODEL: modelling protein tertiary and quaternary structure using evolutionary information. *Nucleic acids research* **42**, W252-258, doi:10.1093/nar/gku340 (2014).

37 McCoy, A. J. *et al.* Phaser crystallographic software. *Journal of applied crystallography* **40**, 658-674, doi:10.1107/S0021889807021206 (2007).

38 Winn, M. D. *et al.* Overview of the CCP4 suite and current developments. *Acta crystallographica. Section D, Biological crystallography* **67**, 235-242, doi:10.1107/S0907444910045749 (2011).

39 Blanc, E. *et al.* Refinement of severely incomplete structures with maximum likelihood in BUSTER-TNT. *Acta crystallographica. Section D, Biological crystallography* **60**, 2210-2221, doi:10.1107/S0907444904016427 (2004).

40 Emsley, P., Lohkamp, B., Scott, W. G. & Cowtan, K. Features and development of Coot. *Acta crystallographica. Section D, Biological crystallography* **66**, 486-501, doi:10.1107/S0907444910007493 (2010).

41 Krissinel, E. & Henrick, K. Inference of macromolecular assemblies from crystalline state. *Journal of molecular biology* **372**, 774-797, doi:10.1016/j.jmb.2007.05.022 (2007).

42 Larkin, M. A. *et al.* Clustal W and Clustal X version 2.0. *Bioinformatics* **23**, 2947-2948, doi:10.1093/bioinformatics/btm404 (2007).

43 Goujon, M. *et al.* A new bioinformatics analysis tools framework at EMBL-EBI. *Nucleic acids research* **38**, W695-699, doi:10.1093/nar/gkq313 (2010).

44 Gouet, P., Courcelle, E., Stuart, D. I. & Metoz, F. ESPript: analysis of multiple sequence alignments in PostScript. *Bioinformatics* **15**, 305-308 (1999).

45 Guindon, S. *et al.* New algorithms and methods to estimate maximum-likelihood phylogenies: assessing the performance of PhyML 3.0. *Systematic biology* **59**, 307-321, doi:10.1093/sysbio/syq010 (2010).

EXTENDED DATA FIGURE LEGENDS:

Extended Data Figure 1. Antibody binding to recombinant ZIKV protein.
a) Biolayer interferometry experiments plotted on a linear scale. The antibodies were immobilized on the biosensor tip, and the ZIKV sE protein was in solution at the indicated concentrations. The antibody used is indicated in each plot. Note that the horizontal scale is different for the three antibodies. The estimated dissociation constant (Kd) and the estimated dissociation rate (Koff) are indicated.
b) Size exclusion chromatography results for isolated sE, isolated Fab fragments, and ZIKV sE + Fab fragments, as indicated.

Extended Data Figure 2. Residues involved in bnAb/antigen interactions.
a) Antibody contacts on the amino acid sequence alignment of ZIKV and DENV-2 sE. A red background highlights identical residues. Secondary structure elements are indicated together with their labels above (ZIKV) and below (DENV-2) the sequences. The domain organization of ZIKV and DENV-2 sE is symbolized by a colored bar above the sequences (domain I red, domain II yellow, domain III blue and the fusion loop orange). Residues involved in polar and van der Waals protein-protein contacts are marked using blue and green symbols, respectively, as indicated in the inset key, displayed above and below the alignment for ZIKV and DENV-2 sE, respectively. Full and empty symbols correspond to antibody contacts on the reference subunit of sE (defined as the one contributing the fusion loop to the epitope) and the opposite subunit of sE, respectively. Residues contacted only by the heavy or light chain are marked with squares or triangles, respectively, and those contacted by both antibody chains with circles. The details of the amino acid contacts are listed in the ED Tables 4 and 5. Dots above the sequences mark every 10 residues on the ZIKV sE sequence. Disulfide bridges are numbered in green above the sequences.
b) Amino acid sequence of the heavy and light chains variable domains (vH and vL) of bnAbs EDE1 C8 (top) and EDE2 A11 (bottom) with the framework (FRW) indicated by black bars and IMGT CDR regions by thin dashed lines. The secondary structure elements of the Ig vH and vL β-barrels are indicated above the sequences. Somatic mutations are in red and residues arising from recombination at the V-D-J junction are in green. Symbols above and below the sequences mark residues involved in contacts with ZIKV and DENV-2 sE, respectively, coded for the contacted site in sE as indicated in the key (inset at the bottom). Polar and van der Waals contacts are shown in blue and green, respectively. The antibody residues contacting the reference sE subunit (defined as the one contributing the fusion loop to the epitope) are marked by plain color symbols while those making contact across the dimer interface by empty colored

symbols. Red boxes highlight the contacts found in the DENV-2 sE complex and absent in the ZIKV sE complex, involving N67 glycan, *kl* and 150 loops. The details of the polar contacts are listed in the Extended Data Tables 4 and 5 (see also Figs 3e and 3f). The predicted vH and vL germline alleles are indicated with the corresponding CDR lengths (see Table 1 in ref. 16).

Extended Data Figure 3. Details of EDE1 C8 bnAb contact across the dimer interface.
a) Overall view of the ZIKV sE/EDE1 C8 scFv complex. The box indicates the region zoomed in b).
b) Details of the interactions of the C8 light chain with domain III across the dimer interface.
c) Same region for the DENV-2 sE/EDE1 C8 Fab complex. Note that the sE residues involved are different.
d) The complex rotated by 120 degrees (as indicated by the arrow) to show the interaction in the *ij* loop, enlarged in e).
e) The *ij* loop is displayed in sticks, in order to show the interaction of its main chain with the antibody. Domain II from the subunit across is colored green to distinguish from domain II of the reference subunit; the dashed sticks for the Arginine shown is to indicate that it has poor electron density in the crystal.
f) Same view of the complex with DENV-2. Note that the residues from across the dimer interface that contact the antibody are different. The residues in the various CDRs are colored coded, matching their label color (as in Figures 3 and 4).

Extended Dta Figure 4. Surface electrostatic potential on an open-book representation of the immmunocomplexes. The electrostatic potential is colored according to the bar underneath. The antibody footprints are outlined in green. The disordered 150 loop in the complex with C8 (left panels) results in a positive surface patch at one edge of the epitope, which is counteracted by the residues in the 150 loop, as shown on the right hand panel, in the complex with A11 where this loop is ordered.

Extended Data Figure 5. Details of the A11 interaction with the glycan on the 150 loop.
a) superposition of the ZIKV sE/A11 complex (in colors) on the E protein from the cryo-EM structure of the mature virion (ref. 5) (PDB code 5IRE) in white. The E-protein was superimposed on the tip of domain II of the reference subunit together with domain III from the opposite subunit. It shows that the 150 loop adopts essentially the same conformation, although fewer sugar residues are visible in the absence of the antibody.

b) Superposition of the ZIKV sE/A11 complex (in colors) on the DENV-2 sE/A11 complex (in white). The variable domains of the antibody from the two structures were superimposed on each other. Note that in DENV-2 the glycan packs against the α-helix of the CDR H3, whereas in ZIKV sE the glycan is too far to make the same interaction.
c) The ZIKV sE/C8 complex (in pink) was superimposed on the ZIKV sE/A11 complex (in colors), to show the clash of the C8 light chain with the glycan, forcing it to move out of the way and be disordered. The superposition also shows that EDE1 C8 reaches further in to contact the *ij* loop and the *kl* loop of the adjacent subunit, as well as domain III. As in a), the superposition was done using the tip of domain II of the reference subunit and domain III of the adjacent subunit in the dimer as anchors. The two black asterisks mark the places where the electron density of the 150 loop is lost, resulting in no density in the ZIKV sE/C8 crystal for the short helix, nor for the glycan.

Figure 1

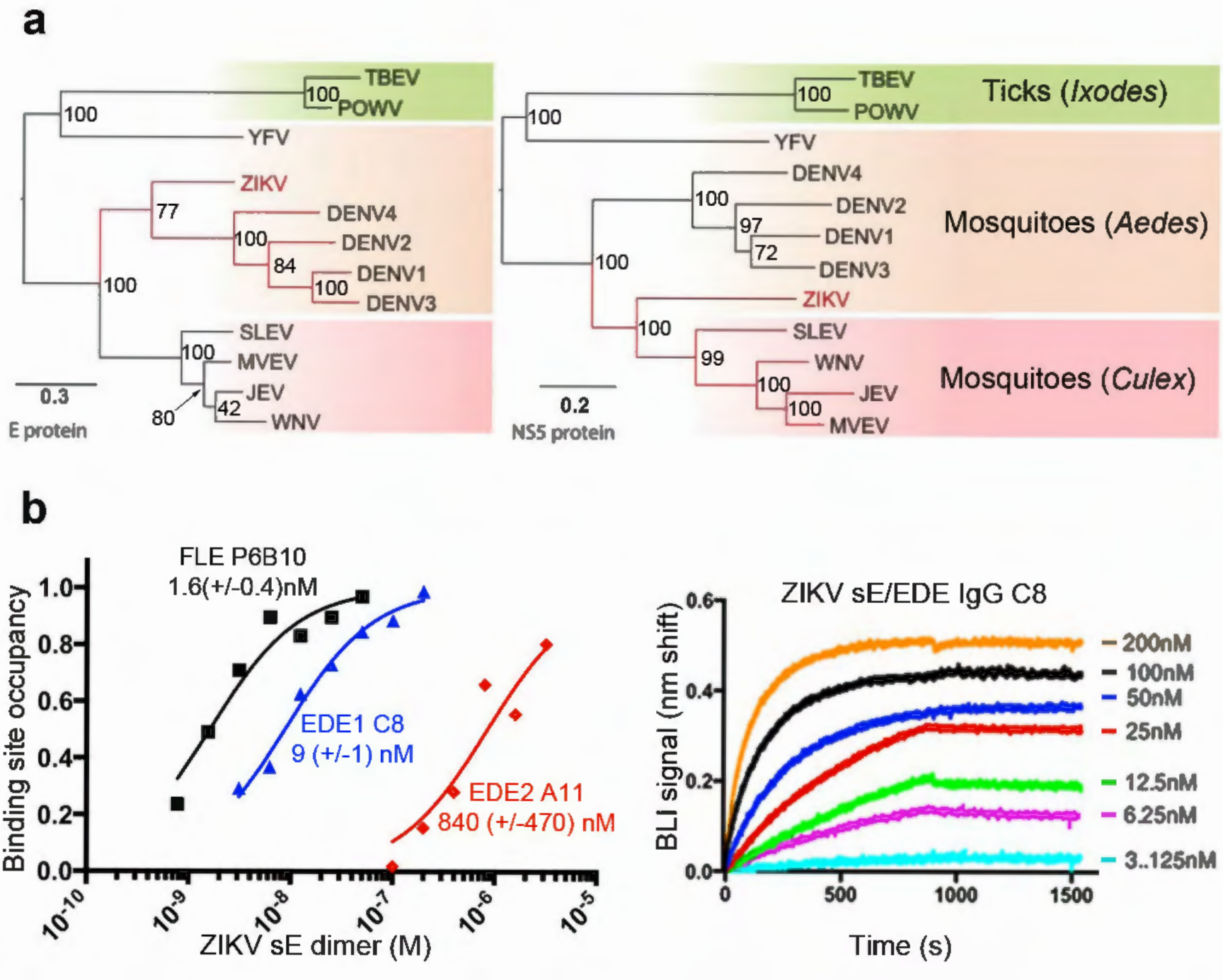
a
TBEV
POWV
YFV
ZIKV
DENV4
DENV2
DENV1
DENV3
SLEV
MVEV
JEV
WNV
100
77
84
80
42
0.3
E protein
Ticks (Ixodes)
Mosquitoes (Aedes)
Mosquitoes (Culex)
97
72
99
0.2
NS5 protein
b
FLE P6B10
1.6(+/-0.4)nM
EDE1 C8
9 (+/-1) nM
EDE2 A11
840 (+/-470) nM
Binding site occupancy
ZIKV sE dimer (M)
ZIKV sE/EDE IgG C8
BLI signal (nm shift)
Time (s)
200nM
100nM
50nM
25nM
12.5nM
6.25nM
3..125nM

Figure 2

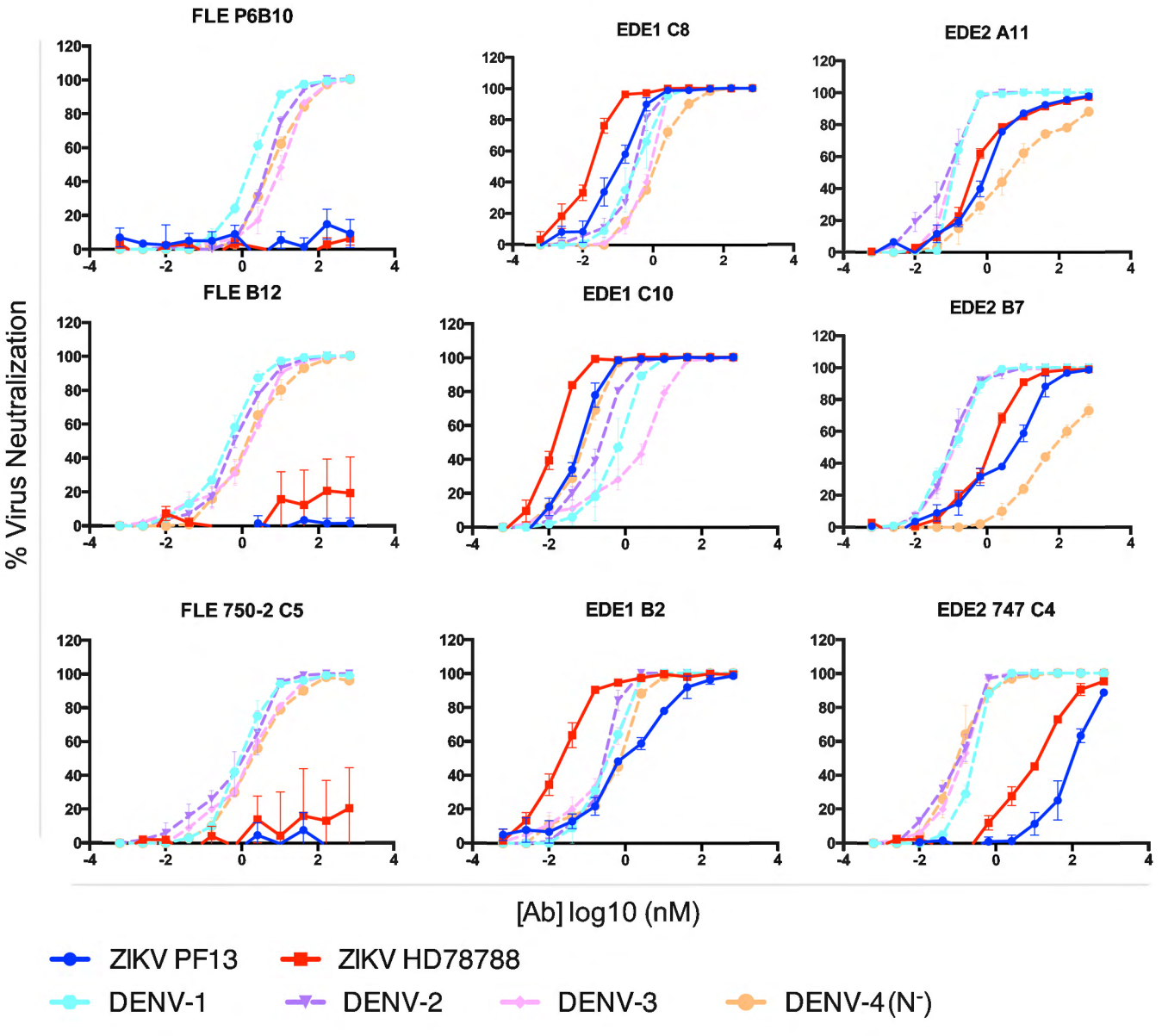
FLE P6B10
EDE1 C8
EDE2 A11
FLE B12
EDE1 C10
EDE2 B7
FLE 750-2 C5
EDE1 B2
EDE2 747 C4
% Virus Neutralization
[Ab] log10 (nM)
ZIKV PF13
ZIKV HD78788
DENV-1
DENV-2
DENV-3
DENV-4 (N-)

Figure 3. Structure of ZIKV sE / EDE1 C8 ScFv complex.

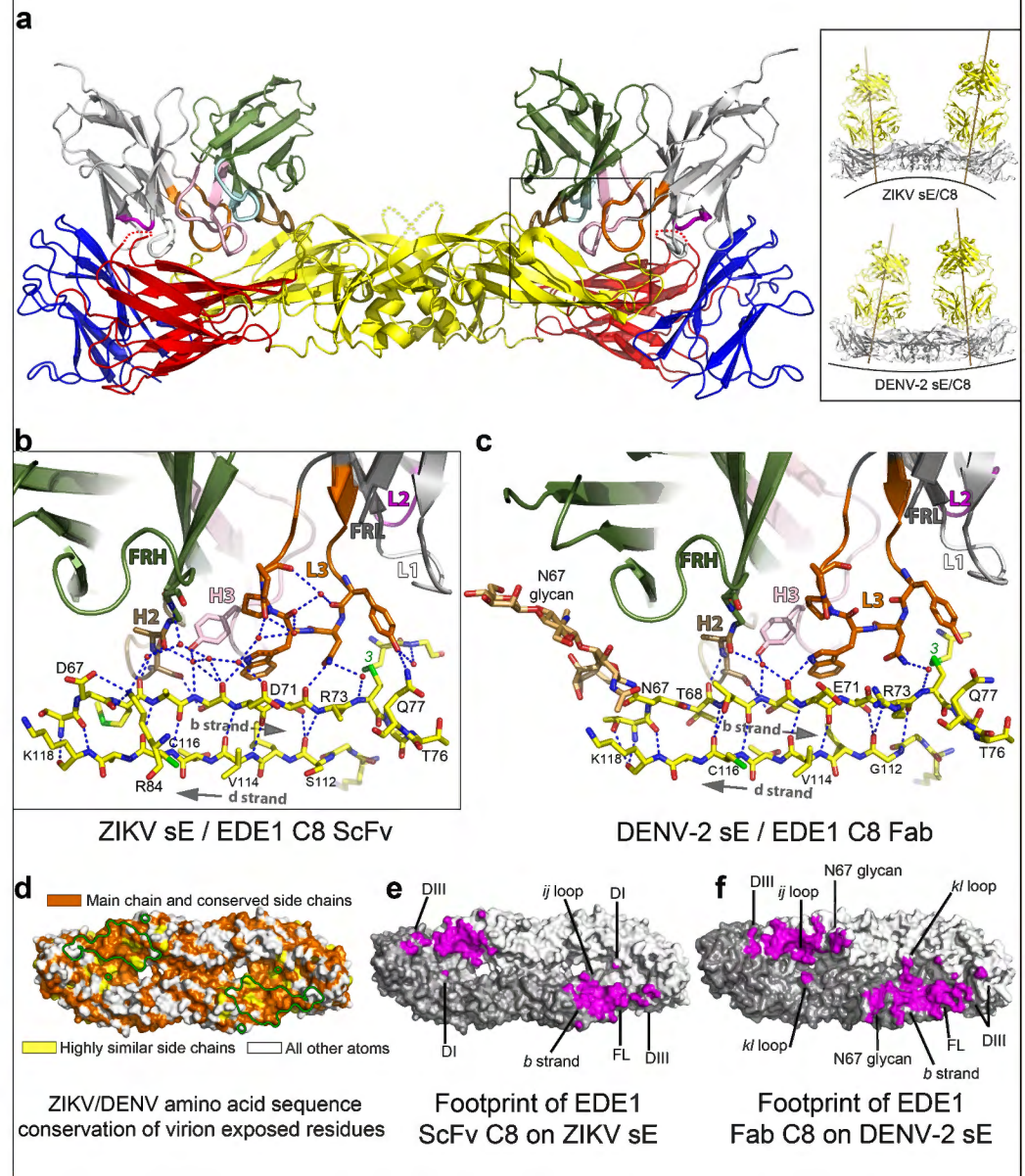

ZIKV sE / EDE1 C8 ScFv

DENV-2 sE / EDE1 C8 Fab

ZIKV/DENV amino acid sequence conservation of virion exposed residues

Footprint of EDE1 ScFv C8 on ZIKV sE

Footprint of EDE1 Fab C8 on DENV-2 sE

Figure 4. Structure of ZIKV sE / EDE2 A11 Fab complex.

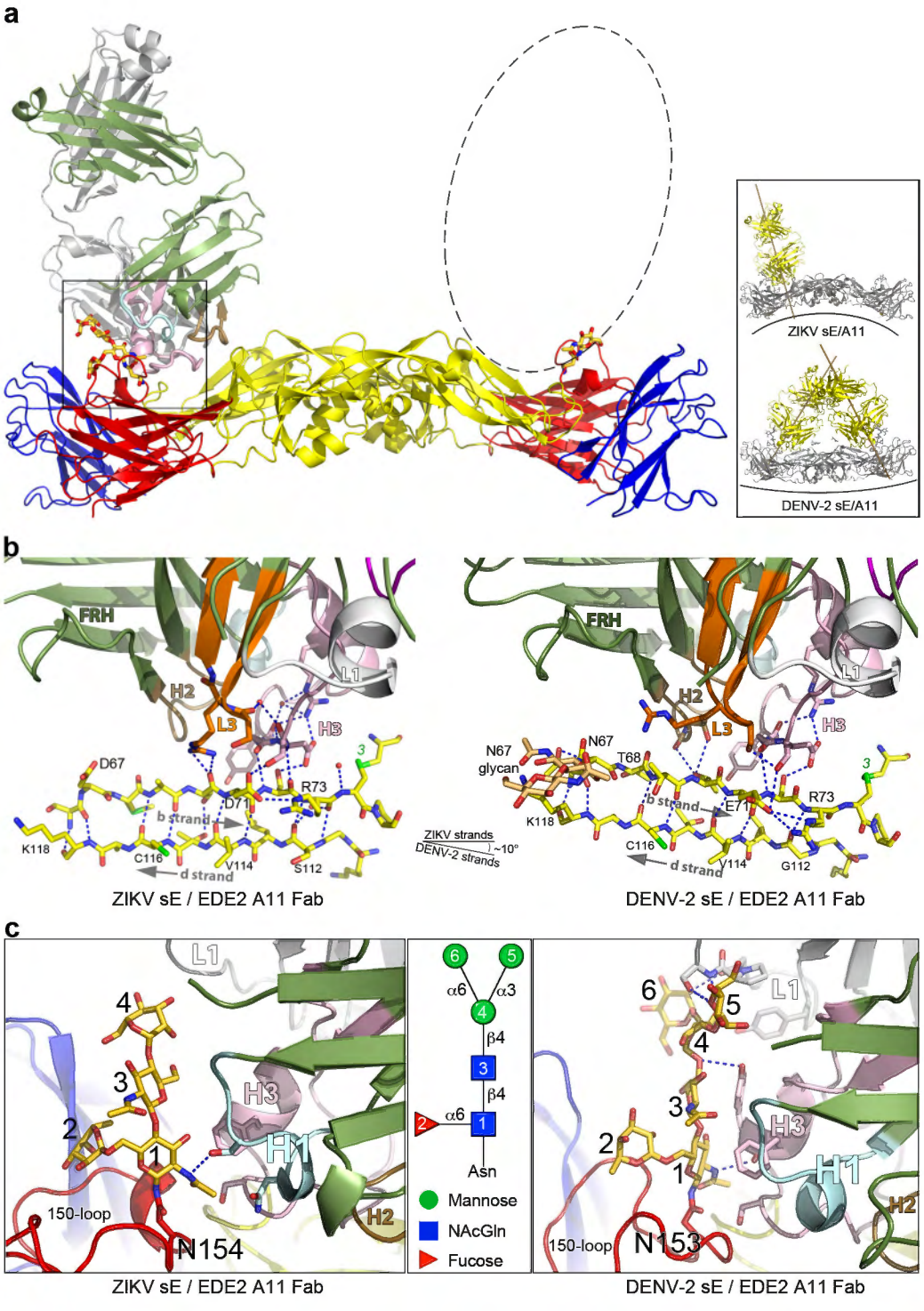

Table 1: 50% FRNT values of EDE1, EDE2, and FLE antibodies tested against ZIKV and DENV 1-4

		ZIKV		DENV			
		50% FRNT (nM)		50% FRNT (nM)			
	Epitope	PF13	HD78788	DENV1	DENV2	DENV3	DENV4
752-2-C8	EDE1	0.095 (±0.026)	0.015 (±0.003)	0.39 (±0.21)	0.24 (±0.06)	0.64 (±0.08)	1.13 (±0.14)
753(3) C10	EDE1	0.063 (±0.016)	0.013 (±0.025)	0.54 (±0.04)	0.18 (±0.02)	1.89 (±0.79)	0.08 (±0.03)
752-2 B2	EDE1	1.062 (±0.362)	0.021 (±0.004)	0.32 (±0.05)	0.23 (±0.02)	0.22 (±0.09)	0.44 (±0.14)
747(4) A11	EDE2	0.904 (±0.191)	0.506 (±0.102)	0.11 (±0.01)	0.07 (±0.03)	0.11 (±0.02)	7.79 (±3.19)
747(4) B7	EDE2	4.31 (±1.47)	1.17 (±0.180)	0.10 (±0.01)	0.11 (±0.02)	0.12 (±0.03)	93.19 (±19.15)
747 C4	EDE2	102 (±25.6)	11.6 (±2.6)	0.23 (±0.02)	0.08 (±0.01)	0.11 (±0.01)	0.12 (±0.05)
758 P6B10	FLE	No Neut.	No Neut.	1.85 (±0.44)	4.97 (±0.28)	9.40 (±2.83)	7.47 (±1.65)
749 B12	FLE	No Neut.	No Neut.	0.43 (±0.12)	0.73 (±0.20)	1.04 (±0.31)	1.80 (±0.64)
750-2 C5	FLE	No Neut.	No Neut.	1.08 (±0.21)	0.76 (±0.46)	1.40 (±0.25)	2.30 (±0.02)

ED Fig. 1

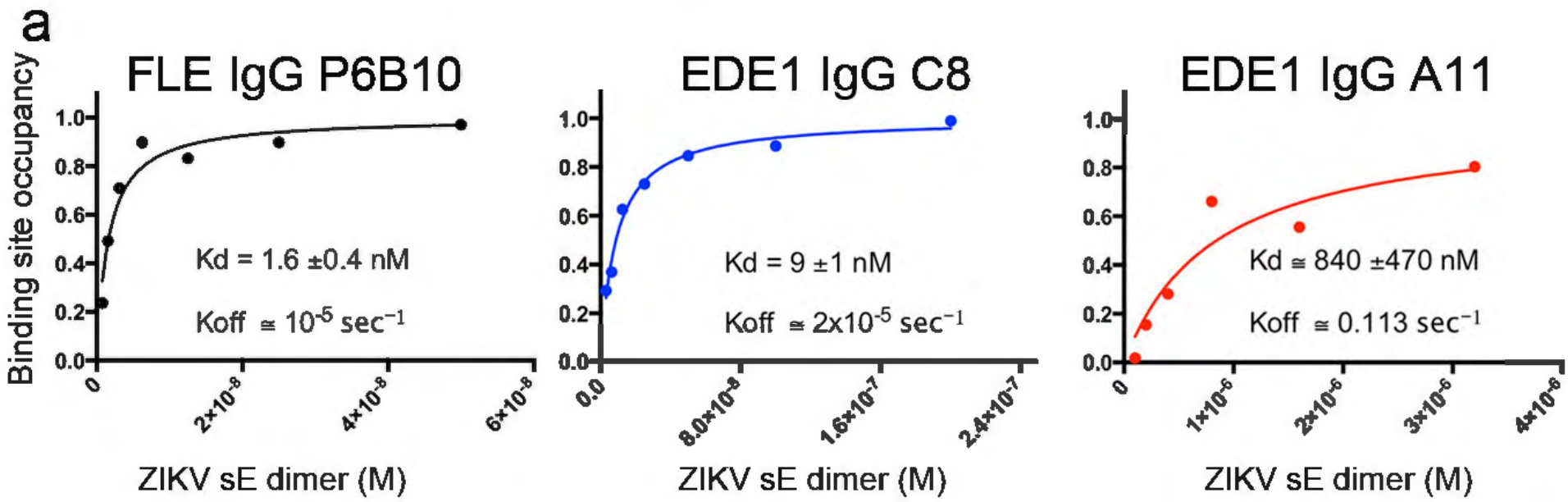
a
FLE IgG P6B10
EDE1 IgG C8
EDE1 IgG A11
Binding site occupancy
Kd = 1.6 ±0.4 nM
Koff ≅ 10-5 sec-1
Kd = 9 ±1 nM
Koff ≅ 2x10-5 sec-1
Kd ≅ 840 ±470 nM
Koff ≅ 0.113 sec-1
ZIKV sE dimer (M)
ZIKV sE dimer (M)
ZIKV sE dimer (M)

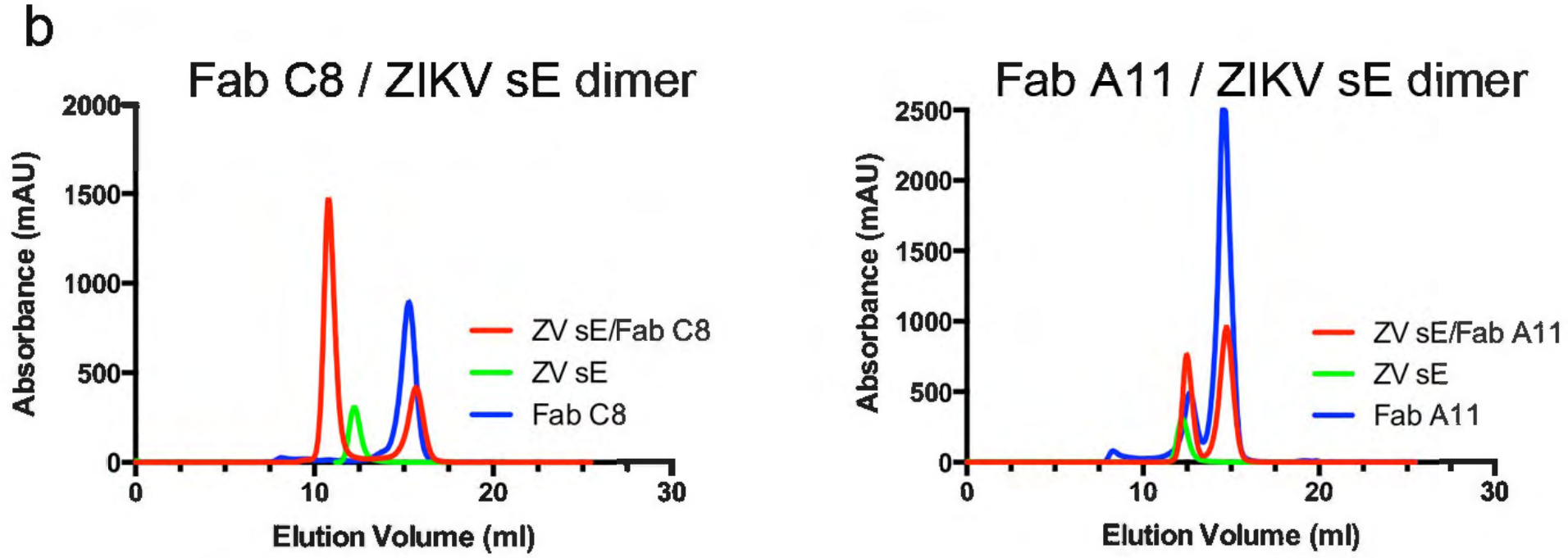
b
Fab C8 / ZIKV sE dimer
Fab A11 / ZIKV sE dimer
Absorbance (mAU)
Elution Volume (ml)
ZV sE/Fab C8
ZV sE
Fab C8
ZV sE/Fab A11
ZV sE
Fab A11

ED Figure 2

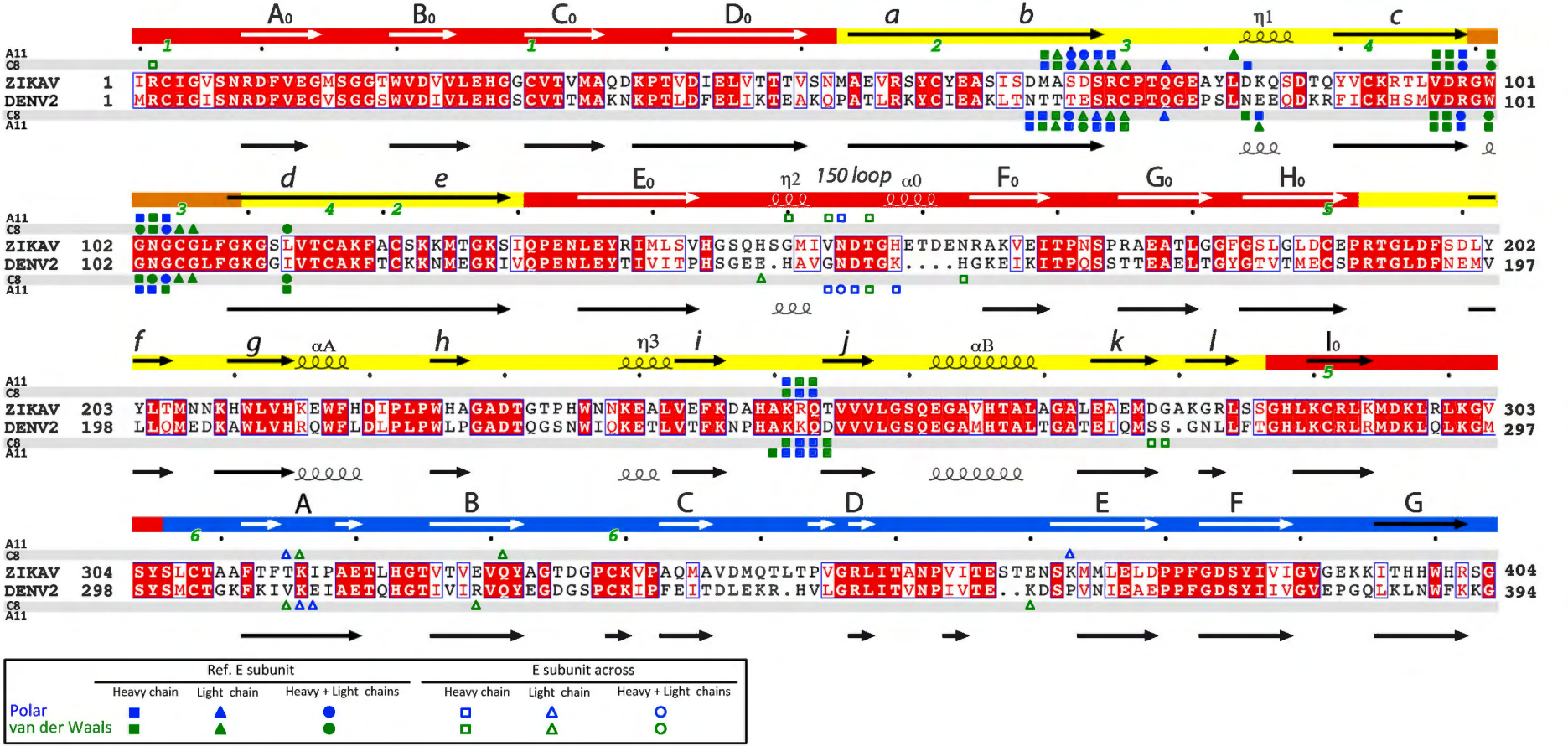
A0 B0 C0 D0 a b η1 c
d e E0 η2 150 loop α0 F0 G0 H0
f g αA h η3 i j αB k l l0
A B C D E F G
A11
C8
ZIKAV 1 IRCIGVSNRDFVEGMSGGTWVDVVLEHGGCVTVMAQDKPTVDIELVTTTVSNMAEVRSYCYEASISDMASDSRCPTQGEAYLDKQSDTQYVCKRTLVDRGW 101
DENV2 1 MRCIGISNRDFVEGVSGGSWVDIVLEHGSCVTTMAKNKPTLDFELIKTEAKQPATLRKYCIEAKLTNTTTESRCPTQGEPSLNEEQDKRFICKHSMVDRGW 101
ZIKAV 102 GNGCGLFGKGSLVTCAKFACSKKMTGKSIQPENLEYRIMLSVHGSQHSGMIVNDTGHETDENRAKVEITPNSPRAEATLGGFGSLGLDCEPRTGLDFSDLY 202
DENV2 102 GNGCGLFGKGGIVTCAKFTCKKNMEGKIVQPENLEYTIVITPHSGEE.HAVGNDTGK....HGKEIKITPQSSTTEAELTGYGTVTMECSPRTGLDFNEMV 197
ZIKAV 203 YLTMNNKHWLVHKEWFHDIPLPWHAGADTGTPHWNNKEALVEFKDAHAKRQTVVVLGSQEGAVHTALAGALEAEMDGAKGRLSSGHLKCRLKMDKLRLKGV 303
DENV2 198 LLQMEDKAWLVHRQWFLDLPLPWLPGADTQGSNWIQKETLVTFKNPHAKKQDVVVLGSQEGAMHTALTGATEIQMSS.GNLLFTGHLKCRLRMDKLQLKGM 297
ZIKAV 304 SYSLCTAAFTFTKIPAETLHGTVTVEVQYAGTDGPCKVPAQMAVDMQTLTPVGRLITANPVITESTENSKMMLELDPPFGDSYIVIGVGEKKITHHWHRSG 404
DENV2 298 SYSMCTGKFKIVKEIAETQHGTIVIRVQYEGDGSPCKIPFEITDLEKR.HVLGRLITVNPIVTE..KDSPVNIEAEPPFGDSYIIVGVEPGQLKLNWFKKG 394
Ref. E subunit
E subunit across
Heavy chain
Light chain
Heavy + Light chains
Polar
van der Waals

ED Fig. 3

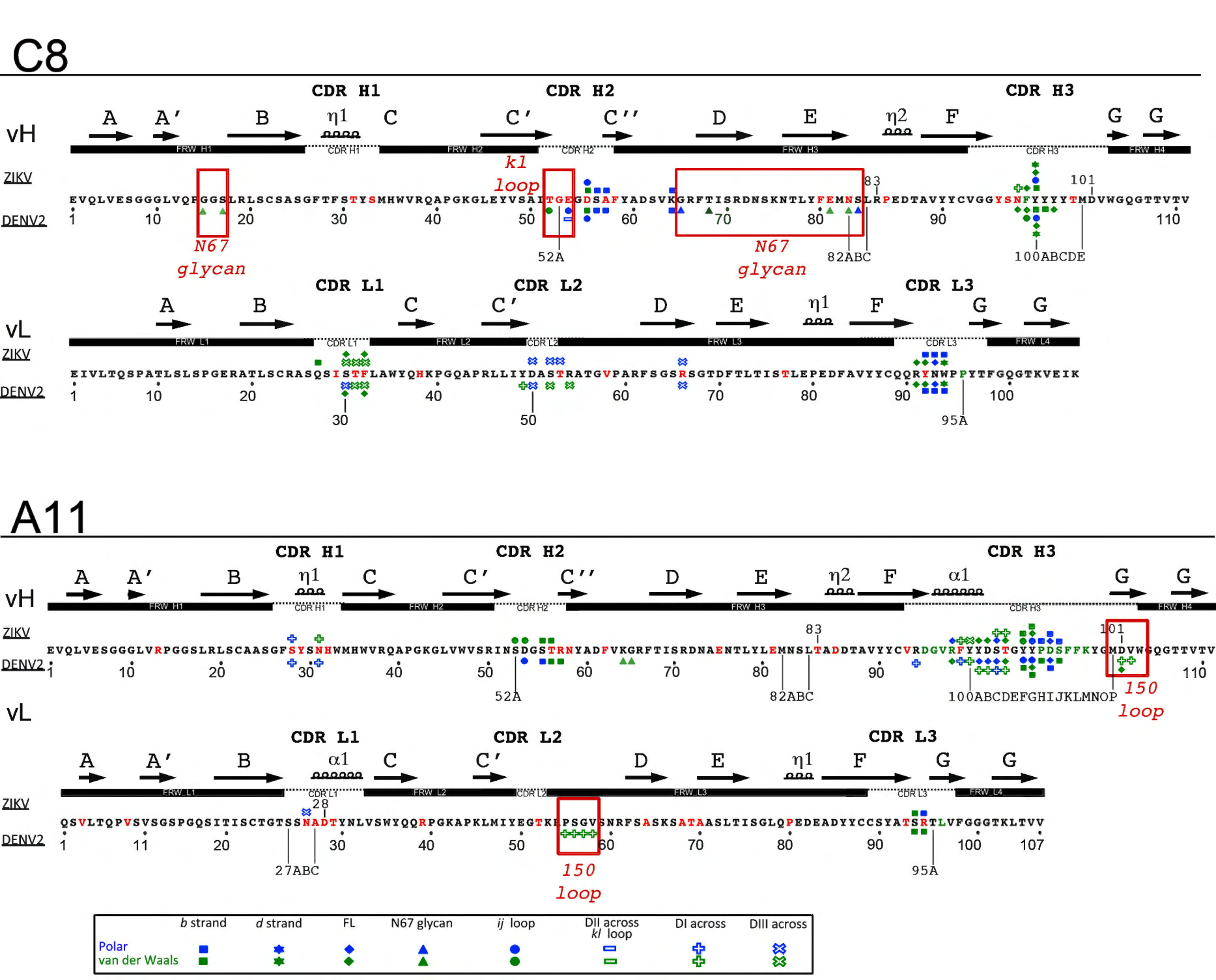
C8
CDR H1
CDR H2
CDR H3
vH
A
A′
B
η1
C
C′
C″
D
E
η2
F
G
G
FRW H1
CDR H1
FRW H2
CDR H2
FRW H3
CDR H3
FRW H4
ZIKV
DENV2
kl loop
N67 glycan
N67 glycan
52A
82ABC
100ABCDE
CDR L1
CDR L2
CDR L3
vL
FRW L1
CDR L1
FRW L2
CDR L2
FRW L3
CDR L3
FRW L4
30
50
95A
A11
α1
150 loop
27ABC
150 loop
b strand
d strand
FL
N67 glycan
ij loop
DII across kl loop
DI across
DIII across
Polar
van der Waals

ED Fig 4

Detailed interactions between ZIKA sE / EDE1 C8 ScFv and DENV-2 sE / EDE1 C8 Fab.

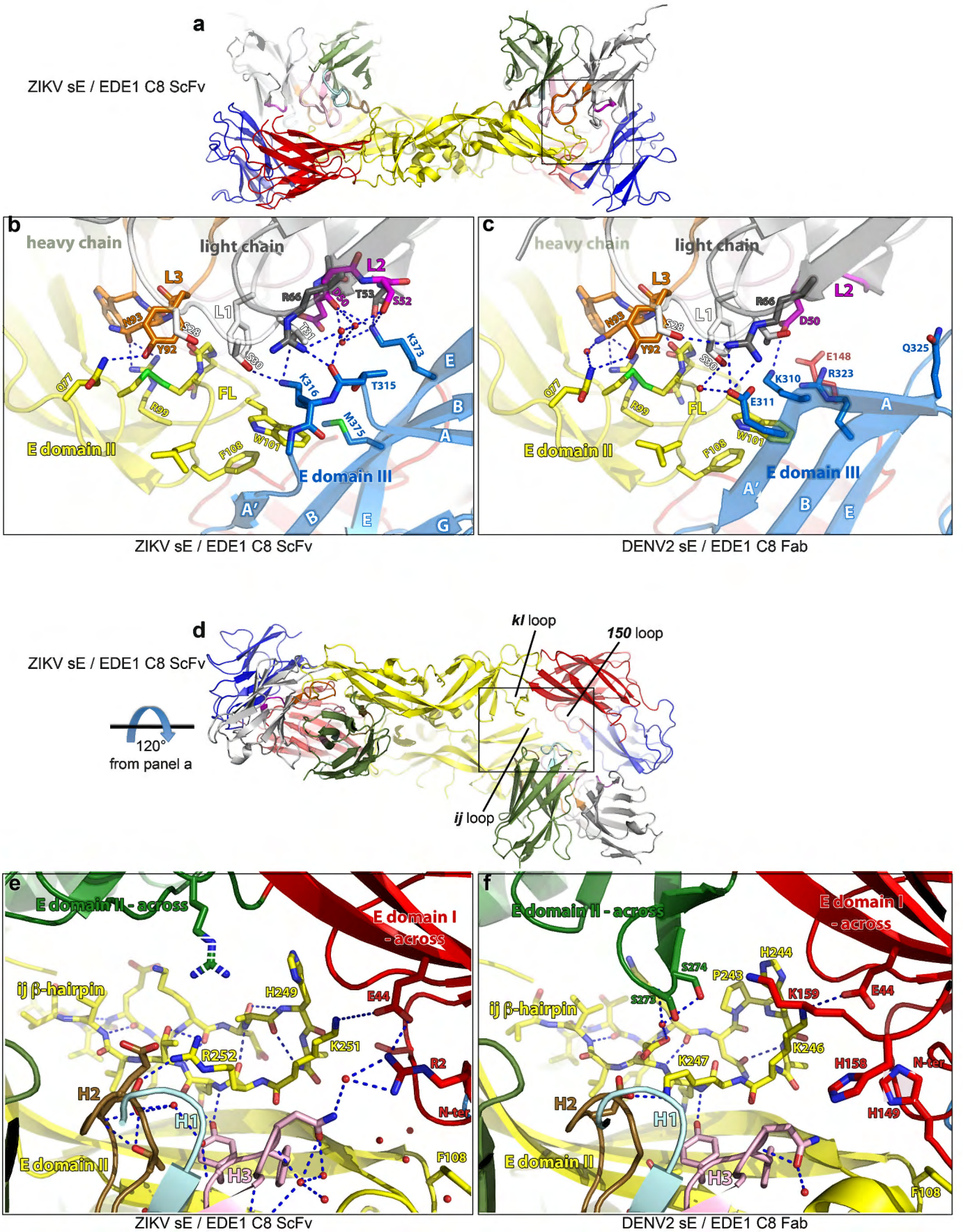

ED Fig. 5

Electrostatic potential of epitopes on ZIKV sE dimers and paratopes on EDE Abs.

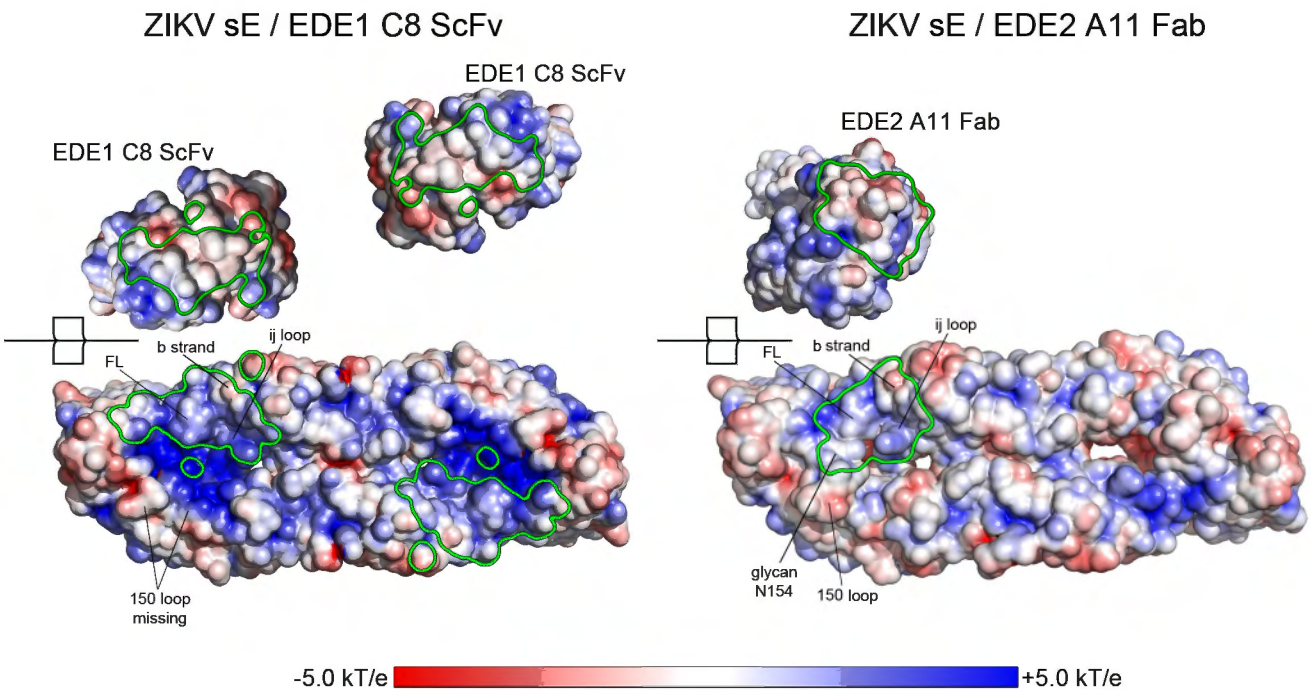

ED Fig. 6

Zoom view of the glycans in ZIKV and DENV-2 complexes with EDE2 A11 Fab and in the ZIKV mature virion.

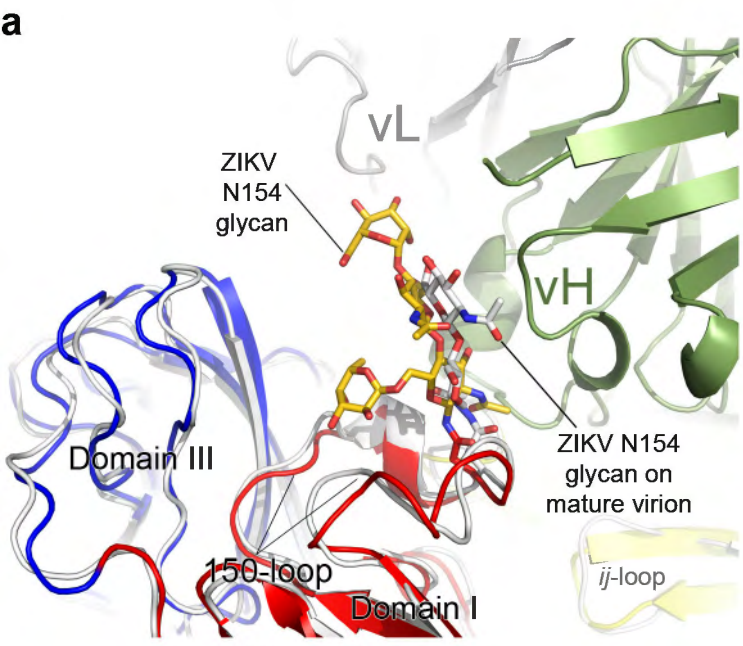

ZIKV sE / EDE2 A11 Fab
ZIKV sE mature virion (5IRE) coloured in white

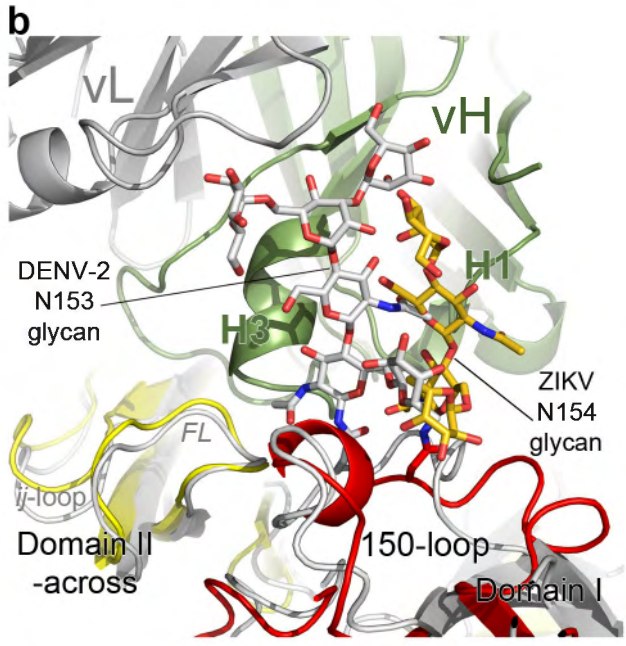

ZIKV sE / EDE2 A11 Fab
DENV-2 sE / EDE2 A11 Fab (4UT7) coloured in white

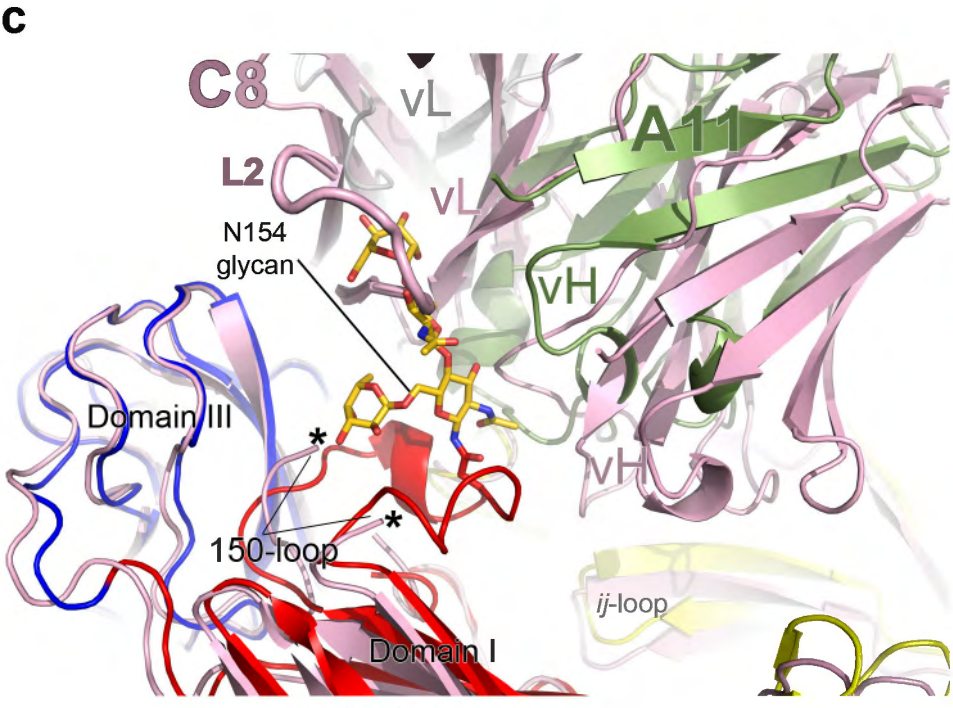

ZIKV sE / EDE2 A11 Fab
ZIKV sE / EDE1 C8 ScFv coloured in pink

Extended Data Table 1. Crystallization conditions, data collection and refinement statistics.

	ZIKV sE / EDE1 C8 ScFv	ZIKV sE / EDE2 A11 Fab	ZIKV sE
Protein Data Bank code	to update	to update	to update
Crystallization conditions			
Protein conc. (mg/ml)*	1.3 (complex)	1.5 (ZIKV sE) 3 (EDE2 A11 Fab)	1,4
Crystallization buffer	1.26 M $(NH_4)_2SO4$, 0.1 M CHES pH 9.5, 0.2 M NaCl	3.5 M Na Formate, 0.1 M Tris pH 8.5	27% PEG 8K, 0.1M Hepes pH 8.3
Crystallization method	sitting drop at 18°C	sitting drop at 18°C	hanging drop at 18°C
Cryo-protectant	20% ethylene glycol in 67% of crystallization solution	16% glycerol in 67% of crystallization solution	16% ethylene glycol in 67% of crystallization solution
Data Collection[$,§]			
Beamline	SOLEIL, Proxima 1	SOLEIL, Proxima 2	ESRF, ID23-2
Detector	Pilatus 6M	Eiger 9M	Pilatus3 2M
Space group	P 2_1 2 2_1	C 2 2 2_1	C 2 2 2_1
Unit cell: a, b, c (Å)	60.8, 121.3, 257.8	204.3, 207.3, 124.6	65.7, 215.3, 124.5
α, β, γ (°)	90, 90, 90	90, 90, 90	90, 90, 90
Resolution (Å)	40.0-**2.41** (2.46-2.41)	40.0-**2.64** (2.69-2.64)	40.0-**3.08** (3.29-3.08)
Anisotropy direction"			
Resolution where $CC_{1/2}$ > 0.50			
overall (Å)	2,69	2,87	**3,08**
along h axis (Å)	3,24	4,23	4,84
along k axis (Å)	2,95	**2,64**	2,99
along l axis (Å)	**2,41**	2,9	3,03
Measured reflections	560 284 (35 314)	760 210 (39 040)	124 201 (23 147)
Unique reflections	74 842 (4571)	77 483 (4 547)	16 828 (3 020)
Completeness (%)	100 (100)	99.8 (99.4)	99.9 (100)
Mn(I) half-set correlation	0.99 (0.15)	0.98 (0.19)	0.99 (0.61)
Mean I/σ(I)	6.7 (1.4)	4.9 (0.4)	7.2 (1.1)
Multiplicity	7.5 (7.7)	9.8 (8.6)	7.4 (7.7)
B wilson ($Å^2$)	31,2	50,4	77,9
Rmerge	0.31 (2.5)	0.51 (6.6)	0.2 (1.9)
Rmeas	0.36 (3.3)	0.52 (6.9)	0.21 (2.1)
Rpim	0.13 (1.2)	0.16 (2.3)	0.08 (0.7)
Structure Determination			
MR search models	ZIKV sE from ZIKV sE / EDE2 A11 Fab complex (this work) EDE1 C8 Fab variable domain (4UTA)	ZIKV model sE from DENV-2 sE (4UTA) EDE2 A11 ScFv (4UT7) EDE2 A11 Fab constant domain (4UTB)	ZIKV sE from refined ZIKV sE / EDE1 C8 ScFv complex
NCS restraint	2	2 applied only on sE dimer	2
Targeting	No targeting	EDE2 A11 Scfv (4UT7)	sE (from ZIKV sE / EDE1 C8 ScFv)
Number of TLS groups	12	12	12
Refinement[§]			
Resolution cut-off (Å)	40.0-**2.41**	40.0-**2.64**	40-**3.08**
Rwork (%) / Rfree (%)	18.7 / 22.0	21.8 / 23.8	22.9 / 27.5
N° of Work / Free reflections	74 785 / 3 719	76 253 / 3 840	16 099 / 843
<B> atomic factors $(Å)^2$	72,6	89,3	142,1
N° of protein atoms	9595	9495	6118
N° of heteroatoms	212	43	0
Rms deviation from ideal			
Bond lengths (Å)	0,01	0,01	0,01
Bond angles (°)	1,22	1,28	1,29
Ramachandran[#]			
Favoured (%)	96,5	93,24	91,92
Allowed (%)	3,26	5,62	4,42
Outliers (%)	0,24	1,14	3,66

The ZIKV sE buffer used for all the crystallization experiments was: 150mM NaCl and 15mM Tris pH 8.

* The protein concentration was estimated using theoretical extinction coefficients of the complexes (ZIKV sE + Fab or scFv), Absorbance at 280nm ($A_{280\ nm}$) of the protein solution was measured before crystallization. The theoretical extinction coefficients for individual component are: ZIKV sE: 1.345; bnAb EDE2 A11 Fab: 1.68 (see Methods for more details); bnAb EDE1 C8 ScFv: 1.9. Extinction coefficients were calculated without taking into account carbohydrate moieties.

One crystal was used to collect a diffraction dataset for each complex to determine the structure.

" The anisotropy statistics were computed with AIMLESS (REF).

[$] Highest resolution shell is shown in parenthesis.

[§] Low-resolution for data processing and refinements was truncated to 40 Å.

[#] Ramachandran statistics were calculated with MolProbity (REF).

Abbreviations used: MR: molecular replacement; NCS: non-crystallographic symetry; TLS: parametrization describing translation, libration and screw-motion to model anisotropic displacements (REF); $CC_{1/2}$: correlation coefficient (REF); h,k and l: indices that define the lattice planes; I/σ(I) empirical signal-to-noise ratio; Rmeas, multiplicity-corrected R; Rpim, expected precision; Rms, root mean square.

Extended Data Table 2. Root mean square deviations between sE dimers in the various structures of ZIKV and DENV-2.

ZIKV[$]		ZIKV sE (this work)	ZIKV sE/ EDE2 A11 Fab	ZIKV sE/ EDE1 C8 ScFv[#]	ZIKV sE (Dai *et al*, 2016)	ZIKV mature virion sE dimer from au	ZIKV mature virion icosahedral sE dimer	ZIKV thermally stable mature virion sE dimer from au	ZIKV thermally stable mature virion icosahedral sE dimer
	PDB code				5JHM	5IRE	5IRE	5IZ7	5IZ7
ZIKV sE (this work)		/							
ZIKV sE/EDE2 A11 Fab		3.33 (796)	/						
ZIKV sE/EDE1 C8 ScFv[#]		2.31 (776) 2.29 (764)	2.41 (773) 2.29 (761)	0.57 (764)[##]					
ZIKV sE (Dai *et al*, 2016)	5JHM	1.8 (769)	4.1 (768)	3.06 (771) 2.93 (761)	/				
ZIKV mature virion sE dimer from au	5IRE	3.22 (800)	1.72 (799)	1.57 (778) 1.69 (764)	3.72 (775)	/			
ZIKV mature virion icosahedral sE dimer	5IRE	2.88 (800)	1.76 (799)	1.60 (778) 1.71 (764)	3.74 (775)	0.46 (806)[1] 0.45 (1002)[2]	/		
ZIKV thermally stable mature virion sE dimer from au	5IZ7	3.03 (800)	1.80 (799)	1.75 (778) 1.88 (764)	3.89 (775)	1.36 (806)[1] 1.57 (1002)[2]	1.36 (806)[1] 1.56 (1002)[2]	/	
ZIKV thermally stable mature virion icosahedral sE dimer	5IZ7	2.94 (800)	1.84 (799)	1.67 (778) 1.80 (764)	3.78 (775)	1.36 (806)[1] 1.56 (1002)[2]	1.36 (806)[1] 1.54 (1002)[2]	1.41 (806)[1] 1.43 (1008)[2]	/

ZIKV/DENV-2[$]		ZIKV sE (this work)	ZIKV sE/ EDE2 A11 Fab	ZIKV sE/ EDE1 C8 ScFv[#]	ZIKV sE (Dai *et al*, 2016)	ZIKV sE mature virion sE dimer from au	ZIKV sE mature virion icosahedral sE dimer	ZIKV thermally stable mature virion sE dimer from au	ZIKV thermally stable mature virion icosahedral sE dimer
	PDB code				5JHM	5IRE	5IRE	5IZ7	5IZ7
DENV-2 sE	4UTC	4.57 (766)	6.47 (768)	5.49 (756) 5.55 (742)	4.75 (753)	5.94 (772)	5.94 (772)	6.23 (757)	6.18 (757)
DENV-2 sE/EDE2 A11 Fab	4UTB	4.45 (773)	7.08 (774) 0.29/0.28 (241)[3]	5.61 (763) 5.57 (744)	4.2 (754)	6.29 (773)	6.28 (773)	7.38 (763)	7.31 (763)
DENV-2 sE/EDE1 C8 Fab	4UTA	6.04 (745)	8.17 (744)	6.88 (748) 6.78 (736)	5.71 (747)	7.52 (751)	7.49 (751)	7.65 (738)	7.57 (738)
DENV-2 mature virion sE dimer from au	3J27	3.89 (779)	2.26 (778)	2.36 (769) 2.81 (755)	4.82 (766)	2.01 (785)[1] 2.09 (979)[2]	2.04 (785)[1] 2.13 (979)[2]	4.33 (770)[1] 2.15 (988)[2]	4.36 (770)[1] 2.20 (988)[2]
DENV-2 mature virion icosahedral sE dimer	3J27	3.59 (779)	2.45 (778)	2.25 (769) 2.68 (755)	4.49 (766)	1.99 (785)[1] 2.07 (979)[2]	1.99 (785)[1] 2.07 (979)[2]	4.31 (770)[1] 2.14 (988)[2]	4.33 (770)[1] 2.15 (988)[2]

DENV-2[$]		DENV-2 sE	DENV-2 sE/ EDE2 A11 Fab	DENV-2 sE/ EDE1 C8 Fab	DENV-2 mature virion sE dimer from au	DENV-2 mature virion icosahedral sE dimer
	PDB code	4UTC	4UTB	4UTA	3J27	3J27
DENV-2 sE	4UTC	/				
DENV-2 sE/EDE2 A11 Fab	4UTB	2.34 (775)	/			
DENV-2 sE/EDE1 C8 Fab	4UTA	2.93 (747)	1.53 (741)	/		
DENV-2 mature virion sE dimer from au	3J27	5.26 (779)	6.78 (775)	6.99 (754)	/	
DENV-2 mature virion icosahedral sE dimer	3J27	4.92 (779)	6.37 (775)	6.56 (754)	0.89 (790)[1] 0.88 (990)[2]	/

rmsd, root mean square deviation (in Å) computed with PyMOL software using the carbon alpha atoms of the sE dimers.
In parenthesis, the number of carbon alpha atoms used for the calculation; PDB code, Protein Data Bank accession number; au, asymetric unit

[$] The rmsd is computed using residues 1 to 403 for ZIKV sE or residues 1 to 395 for DENV-2 sE, except when indicated[1,2].
[#] There are two independent half dimer (ZIKV sE/EDE1 C8 ScFv) in the asymetric unit.
The rmsd is computed between the two dimers of sE generated by crystallographic symetry for each sE in the asymetric unit.
[##] This rmsd is computed between the two independent half dimers of sE in the asymetric unit.
[1] The rmsd is computed between the sE dimers excluding stem and TM regions of ZIKV (residues 1 to 403) and DENV-2 (residues 1 to 395).
[2] The rmsd is computed between the sE dimers including stem and TM regions of ZIKV and DENV-2 (residues 1 to C terminal).
[3] The two rmsd values refer to the superposition of the variable domains of Fab A11 in ZIKV sE/EDE2 A11 Fab on each Fab A11 in DENV-2 sE/EDE2 A11 Fab.

	BSA BNA Fab or ScFv			BSA sE dimer					Complex	
	vH	vL	Total	Reference subunit (glycans[#])	Opposite subunit (glycans[#])	Total	Main chain atoms[‡]	Total glycan BSA[€]	BSA / molecule	SC
ZIKV sE / EDE1 C8 ScFv fragment*										
ZIKV sE dimer Epitope dimer-1	426.1	494.8	920.9	653.0 (NA)	237.2 (NA)	890.2	346.9 (39%)	NA	905.5	0.683
ZIKV sE dimer Epitope dimer-2	438.4	492.4	930.8	678.1 (NA)	223.2 (NA)	901.3	343.9 (38%)	NA	916.0	0.738
DENV-2 sE / EDE1 C8 Fab fragment (4UTA)										
DENV-2 sE dimer Epitope A	718.9 (516.8)"	471.0 (471.0)"	1189.9	919.1 (192.9)	222.2	1141.3	357.8 (31%)	192.9 (17%)	1165.6	0.693
DENV-2 sE dimer Epitope B	831.9 (570.3)"	528.3 (528.3)"	1360.2	945.5 (230.9)	340.0	1285.5	359.0 (28%)	230.9 (18%)	1322.8	0.687
ZIKV sE / EDE2 A11 Fab fragment[£]										
ZIKV sE dimer Epitope	718.5	75.7	793.4	570.0 (0.0)	217.4 (134.6)	787.4	253.7 (32.2%)	134.6 (17%)	790.4	0.674
DENV-2 sE / EDE2 A11 Fab fragment (4UTB)										
DENV-2 sE dimer Epitope A	923.9 (251.3)	189.2 (148.8)	1113.0	531.8 (14.2)	472.6 (342.4)	1004.4	221.5 (22%)	356.6 (35%)	1058.7	0.706
DENV-2 sE dimer Epitope B	954.1 (302.2)	185.1 (136.7)	1138.8	460.3 (58.5)	571.3 (341.4)	1031.6	219.3 (21.2%)	400.0 (39%)	1085.2	0.668

BSA, buried surface area (in $Å^2$) of sE protein by the Fabs or ScFv (calculated with the program 'areaimol' in CCP4).
BSA/molecule, average buried surface area between one Fab or one ScFv and the sE dimer.

SC, shape complementarity coefficient (calculated with the program 'sc' in CCP4).

The dots density used to compute both BSA and SC was set to 15 dots/$Å^2$. The van der Waals prode radius was set to 1.4 Å.
NA, Non applicable.

[#] In parenthesis, contribution of glycan chains to buried surface area : N154 (for ZIKV sE) and N67 and/or N153 (for DENV-2 sE).

" In parenthesis, the BSA was computed removing the glycan chains N67 for DENV-2 sE, in order to compare with the BSA of ZIKV sE which do not carry the N67 glycan.

[‡] Contribution of main-chain atoms to buried surface area; In parenthesis, contribution indicated as percentages.

* There are two independent half dimer (ZIKV sE / EDE1 C8 ScFv) in the asymetric unit.
The two dimers of ZIKV sE (dimer-1 and dimer-2) are generated by applying crystallographic symetry for each sE in the asymetric unit.

[£] Only one Fab A11 binds to the sE dimer in ZIKV sE / EDE2 A11 Fab complex.

Extended Data Table 4. Polar and salt bridges interactions for ZIKV sE/EDE1 C8 ScFv, ZIKV sE/EDE2 A11 Fab, DENV-2 sE/EDE1 C8 Fab and DENV-2 sE/EDE2 A11 Fab.

domains of sE		ZIKV sE / EDE2 Fab A11				DENV-2 sE / EDE2 Fab A11 (4UTB) epitope A				DENV-2 sE / EDE2 Fab A11 (4UTB) epitope B			
		sE	dist (Å)	Fab A11	CDR	sE	dist (Å)	Fab A11	CDR	sE	dist (Å)	Fab A11	CDR
domain I - Reference subunit	b-strand	S 70 [O]	2.96	R 95 [NH1]	L3								
		S 70 [O]	2.96	R 95 [NH2]	L3								
						T 70 [OG1]	3.53	S 55 [O]	H2	T 70 [OG1]	3.42	S 55 [O]	H3
		D 71 [OD1]	**3.72**	**R 95 [NH1]**	**L3**								
		D 71 [OD1]	2.66	S 100J [OG]	H3								
		S 72 [OG]	3.21	D 100I [N]	H3	S 72 [OG]	3.73	D 100I [N]	H3	S 72 [OG]	3.61	D 100I [N]	H3
		S 72 [OG]	2.71	D 100I [OD1]	H3	S 72 [OG]	2.78	D 100I [OD1]	H3	S 72 [OG]	3.01	D 100I [OD1]	H3
		S 72 [O]	3.49	S 100J [N]	H3					S 72 [O]	3.69	S 100J [N]	H3
		S 72 [N]	3.39	P 100H [O]	H3					S 72 [N]	3.45	P 100H [O]	H3
		R 73 [N]	3.44	D 100I [OD1]	H3								
		R 73 [NE]	2.83	S 100J [OG]	H3					R 73 [NE]	3.59	S 100J [OG]	H3
	Fusion loop					D 98 [O]	3.51	Y 100G [OH]	H3				
		R 99 [NH1]	**2.78**	**D 100I [OD1]**	**H3**								
		R 99 [NH1]	**3.47**	**D 100I [OD2]**	**H3**								
		R 99 [NH2]	**3.60**	**D 100I [OD1]**	**H3**	**R 99 [NH2]**	**2.64**	**D 100I [OD2]**	**H3**	**R 99 [NH2]**	**2.76**	**D 100I [OD1]**	**H3**
		R 99 [NH2]	**2.70**	**D 100I [OD2]**	**H3**	**R 99 [NH2]**	**2.83**	**D 100I [OD1]**	**H3**	**R 99 [NH2]**	**2.49**	**D 100I [OD1]**	**H3**
		G 102 [O]	3.16	S 100C [N]	H3	G 102 [O]	3.49	S 100C [N]	H3	G 102 [O]	3.83	S 100C [N]	H3
		G 102 [O]	3.25	S 100C [OG]	H3	G 102 [O]	2.88	S 100C [OG]	H3	G 102 [O]	3.02	S 100C [OG]	H3
						N 103 [N]	3.84	Y 100A [O]	H3				
		G 104 [O]	3.78	R 98 [NH1]	H3								
	ij loop	K 251 [O]	2.72	Y 100G [OH]	H3	K 246 [O]	2.77	Y 100G [OH]	H3	K 246 [O]	2.76	Y 100G [O]	H3
						K 247 [NZ]	**3.39**	**D 53 [OD1]**	**H2**				
						K 247 [NZ]	**3.7**	**D 53 [OD2]**	**H2**				
						Q 248 [O]	3.23	Y 100F [O]	H3	Q 248 [O]	3.70	Y 100F [OH]	H3
						Q 248 [N]	3.18	Y 100F [OH]	H3	Q 248 [N]	3.85	Y 100F [OH]	H3
	N67 glycan	no glycan at this position											
	dom III	P 354 [O]	3.71	N 27B [ND2]	L1								
domain I - across	150 loop	V 153 [O]	3.5	S 100C [OG]	H3	G 152 [O]	3.62	S 100C [OG]	H3				
						D 154 [OD2]	2.79	N 31 [ND2]	H1	D 154 [OD2]	3.64	N 31 [ND2]	H1
						D 154 [N]	3.17	S 100C [OG]	H3	D 154 [N]	3.35	S 100C [OG]	H3
						K 157 [NZ]	3.34	S 28 [OG]	H1	K 157 [NZ]	3.20	S 28 [OG]	H1
	N153/ N154 glycan	N154-1 [N2]	3.37	S 28 [OG]	H1	N153-1 [N2]	3.43	F 99 [O]	H3	N153-1 [N2]	3.28	F 99 [O]	H3
		N154-1 [O3]	3.09	S 28 [OG]	H1								
										N153-3 [O3]	3.86	Y 100 [OH]	H3
						N153-4 [O3]	3.89	Y 100 [OH]	H3				
						N153-4 [O4]	2.86	S 56 [OG]	L2				
						N153-4 [O4]	3.64	S 56 [N]	L2	N153-4 [O4]	3.08	S 56 [N]	L2
						N153-4 [O6]	3.69	S 56 [N]	L2	N153-4 [O6]	3.55	S 56 [N]	L2
						N153-4 [O3]	3.89	Y 100 [OH]	H3				
						N153-6 [O2]	3.54	R 94 [NH2]	H3	N153-6 [O2]	3.81	R 94 [NH2]	H3
										N153-6 [O5]	3.34	S 56 [OG]	L2

		ZIKV sE / EDE1 ScFv C8				DENV-2 sE / EDE1 Fab C8 (4UTA) epitope A				DENV-2 sE / EDE1 Fab C8 (4UTA) epitope B			
		sE	dist (Å)	ScFv C8	CDR	sE	dist (Å)	Fab C8	CDR	sE	dist (Å)	Fab C8	CDR
domain II - reference subunit	b-strand	M 68 [O]	3.72	S 5 [OG]	H2	T 68 [O]	3.11	A 57 [N]	H2	T 68[O]	3.11	A 57 [N]	H1
		M 68 [O]	3.22	A 57 [N]	H2								
		S 70 [OG]	2.94	S 56 [OG]	H2	T 70 [OG1]	2.96	S 56 [OG]	H2	T 70 [OG1]	3.1	S 56 [OG]	H1
		S 70 [N]	3.14	S 56 [OG]	H2	T 70 [N]	3.23	S 56 [OG]	H2	T 70 [N]	3.14	S 56 [OG]	H1
		S 70 [O]	3.14	W 94 [NE1]	L3	T 70 [O]	2.76	W 94 [NE1]	L3	T 70 [O]	2.8	W 94 [NE1]	L3
		S 72 [O]	3.12	N 93 [ND2]	L3	S 72 [O]	3.48	N 93 [ND2]	L3				
		Q 77 [NE2]	3.34	Y 92 [OH]	L3	Q 77 [NE2]	3.46	Y 92 [OH]	L3				
		D 83 [OD1]	**3.56**	**K 64 [NZ]**	**FH3**								
						E 84 [OE1]	**3.67**	**K 64 [NZ]**	**H2**	**E 84 [OE2]**	**3.94**	**K 64 [NZ]**	**H2**
						E 84 [OE2]	**3.71**	**K 64 [NZ]**	**H2**	**E 84 [OE1]**	**3.83**	**K 64 [NZ]**	**H2**
	Fusion loop	R 99 [NH2]	3.65	N 93 [O]	L3								
		R 99 [NH1]	2.87	N 93 [OD1]	L3	R 99 [NH1]	3.1	N 93 [OD1]	L3	R 99 [NH1]	2.96	N 93 [OD1]	L3
		R 99 [NH2]	3.02	N 93 [OD1]	L3	R 99 [NH2]	2.98	N 93 [OD1]	L3	R 99 [NH2]	2.89	N 93 [OD1]	L3
		G 104 [O]	2.74	N 93 [N]	L3	G 104 [O]	2.86	N 93 [N]	L3	G 104 [O]	2.93	N 93 [N]	L3
	ij loop	**R 252 [NH2]**	**3.37**	**D 55 [OD2]**	**H2**	**K 247 [NZ]**	**2.75**	**D 55 [OD2]**	**H2**	**K 247[NZ]**	**2.78**	**D 55 [OD2]**	**H2**
						K 247 [NZ]	**3.84**	**E 53 [OE1]**	**H2**				
		Q 253 [N]	3.11	Y 100 [OH]	H3	Q 248 [N]	3.03	Y 100 [OH]	H3	Q 248 [N]	2.97	Y 100 [OH]	H3
		Q 253 [O]	3.37	Y 100 [OH]	H3					Q 248 [O]	3.5	Y 100 [OH]	H3
	N67 glycan	non existing glycan				N67-1 [O3]	3	G 65 [O]	H2	N67-1 [O3]	3.0	G 65 [O]	H2
						N67-4 [O2]	2.7	S 82B [OG]	FH3	N67-4 [O2]	3.32	S 82B [OG]	FH3
	150 loop	disordered loop				disordered loop				disordered loop			
	N153/ N154 glycan	disordered glycan				disordered glycan				disordered glycan			
domain I - across	*kl* loop	disordered loop				disordered loop				S 274 [N]	3.3	E 53 [OE2]	H1
domain III - across	A strand					**K 310 [NZ]**	**3.69**	**D 50 [OD1]**	**L2**	**K 310 [NZ]**	**3.62**	**D 50 [OD1]**	**L2**
						E 311 [OE1]	**3.94**	**R 66 [NH1]**	**FL3**	**E 311 [OE1]**	**3.35**	**R 66 [NH1]**	**FL3**
						E 311 [OE2]	**2.74**	**R 66 [NH1]**	**FL3**	**E 311 [OE1]**	**3.65**	**R 66 [NH2]**	**FL3**
						E 311 [OE2]	**3.28**	**R 66 [NH2]**	**FL3**	**E 311 [OE2]**	**2.8**	**R 66 [NH1]**	**FL3**
						E 311 [OE1]	3.28	S 30 [OG]	FL1				
		T 315 [O]	2.58	R 66 [NH1]	FL3								
						D 362 [OD2]	**3.69**	**R 54 [NH1]**	**L2**				
	E strand	K 373 [NZ]	2.85	S 52 [OG]	L2								
		K 373 [NZ]	2.98	T 53 [OG]	L2								
		K 373 [NZ]	3.56	D 50 [O]	L2								

The polar contacts were computed with PISA server (REF).
In bold red: main chain atoms involved in contacts; In bold black: salt bridges; In bold blue: glycan interactions
Hydrogen bonds distances cut-off: 3.5Å; Salt bridges distances cut-off: ≤ 4Å

Extended Data Table 5. Polar and salt bridges interactions for ZIKV sE/EDE1 C8 ScFv, ZIKV sE/EDE2 A11 Fab, DENV-2 sE/EDE1 C8 Fab and DENV-2 sE/EDE2 A11 Fab.

			ZIKV sE / EDE2 Fab A11				DENV-2 sE / EDE2 Fab A11 (4UTB) epitope A				DENV-2 sE / EDE2 Fab A11 (4UTB) epitope B			
	CDR	sE	sE	dist (Å)	Fab A11	CDR	sE	dist (Å)	Fab A11	CDR	sE	dist (Å)	Fab A11	CDR
Light chain	L1	dom III	P 354 [O]	3.71	N 27B [ND2]	L1								
	L2	domain I - across N154 glycan					N153-4 [O4] N153-4 [O4] N153-4 [O6]	2.86 3.64 3.69	S 56 [OG] **S 56 [N]** **S 56 [N]**	L2 L2 L2	N153-4 [O4] N153-4 [O6] N153-6 [O5]	3.08 3.55 3.34	**S 56 [N]** **S 56 [N]** S 56 [OG]	L2 L2 L2
	L3	b-strand	**S 70 [O]** **D 71 [OD1]**	2.84 **3.75**	R 95 [NH1] **R 95 [NH1]**	L3 L3								
Heavy chain	H1	domain I - across N154 glycan	N154-1 [N2] N154-1 [O3]	3.24 3.03	S 28 [OG] S 28 [OG]	H1 H1								
		150 loop					D 154 [OD2] K 157 [NZ]	2.79 3.34	N 31 [ND2] S 28 [OG]		D 154 [OD2] K 157 [NZ]	3.64 3.20	N 31 [ND2] S 28 [OG]	H1 H1
	H2	*ij*-loop					**K 247 [NZ]** **K 247 [NZ]**	**3.39** **3.7**	**D 53 [OD1]** **D 53 [OD2]**					
		b-strand					T 70 [OG1]	3.5	**S 55 [O]**	H2	T 70 [OG1]	3.42	**S 55 [O]**	H2
			S 72 [OG] S 72 [OG] **S 72 [O]** **S 72 [N]** **R 73 [N]** R 73 [NE]	3.30 2.69 3.50 3.43 3.45 2.83	**D 100I [N]** D 100I [OD1] **S 100J [N]** **P 100H [O]** D 100I [OD1] S 100J [OG]	H3 H3 H3 H3 H3 H3	S 72 [OG] S 72 [OG]	3.73 2.78	**D 100I [N]** D 100I [OD1]	H3 H3	S 72 [OG] S 72 [OG] **S 72 [O]** **S 72 N]** R 73 [NE]	3.61 3.01 3.69 3.45 3.59	**D 100I [N]** D 100I [OD1] **S 100J [N]** **P 100H [O]** S 100J [OG]	H3 H3 H3 H3 H3
		Fusion loop					**D 98 [O]**	3.51	Y 100G [OH]	H3				
			R 99 [NH1] **R 99 [NH1]** **R 99 [NH2]** **R 99 [NH2]** **G 102 [O]** **G 102 [O]**	**2.83** **3.5** **3.64** **2.74** 3.16 3.20	**D 100I [OD1]** **D 100I [OD2]** **D 100I [OD1]** **D 100I [OD2]** **S 100C [N]** S 100C [OG]	H3 H3 H3 H3 H3 H3	**R 99 [NH2]** **R 99 [NH2]** **G 102 [O]** **G 102 [O]** **N 103 [N]**	**2.64** **2.83** 3.49 2.88 3.84	**D 100I [OD2]** **D 100I [OD1]** **S 100C [N]** S 100C [OG] **Y 100A [O]**	H3 H3 H3 H3 H3	**R 99 [NH2]** **R 99 [NH2]** **G 102 [O]** **G 102 [O]**	**2.76** **2.49** 3.83 3.02	**D 100I [OD1]** **D 100I [OD1]** **S 100C [N]** S 100C [OG]	H3 H3 H3 H3
			G 104 [O]	3.84	R 98 [NH1]	H3								
		ij-loop	**K 251 [O]**	2.83	Y 100G [OH]	H3	**K 246 [O]** **Q 248 [O]** **Q 248 [N]**	2.77 3.23 3.18	Y 100G [OH] Y 100F [O] Y 100F [OH]	H3 H3 H3	**K 246 [O]** **Q 248 [O]** **Q 248 [N]**	2.76 3.70 3.85	Y 100G [O] Y 100F [OH] Y 100F [OH]	H3 H3 H3
		150 loop	**V 153 [O]**	3.5	S 100C [OG]	H3	**G 152 [O]** **D 154 [N]**	3.62 3.17	S 100C [OG] S 100C [OG]	H3 H3	**D 154 [N]**	3.35	S 100C [OG]	H3
		N153/ N154 glycan					**N153-1 [N2]**	3.43	**F 99 [O]**	H3	**N153-1 [N2]** **N153-3 [O3]**	3.28 3.86	**F 99 [O]** Y 100 [OH]	H3 H3
							N153-4 [O3] **N153-4 [O3]**	3.89 3.89	Y 100 [OH] Y 100 [OH]	H3 H3				
							N153-6 [O2]	3.54	R 94 [NH2]	H3	**N153-6 [O2]**	3.81	R 94 [NH2]	H3

			ZIKV sE / EDE1 ScFv C8				DENV-2 sE / EDE1 Fab C8 (4UTA) epitope A				DENV-2 sE / EDE1 Fab C8 (4UTA) epitope B			
	CDR	sE	sE	dist (Å)	ScFv C8	CDR	sE	dist (Å)	Fab C8	CDR	sE	dist (Å)	Fab C8	CDR
Light chain	FL1	dom III - across A strand					E 311 [OE1]	3.28	S 30 [OG]	FL1	E 311 [OE1]	3.28	S 30 [OG]	FL1
	FL3		**T 315 [O]**	2.58	R 66 [NH1]	FL3	**E 311 [OE1]** **E 311 [OE2]** **E 311 [OE2]**	**3.94** **2.74** **3.28**	**R 66 [NH1]** **R 66 [NH1]** **R 66 [NH2]**	FL3 FL3 FL3	**E 311 [OE1]** **E 311 [OE2]** **E 311 [OE2]**	**3.94** **2.74** **3.28**	**R 66 [NH1]** **R 66 [NH1]** **R 66 [NH2]**	FL3 FL3 FL3
	L2	A strand					**K 310 [NZ]**	**3.69**	**D 50 [OD1]**	L2	**K 310 [NZ]**	**3.69**	**D 50 [OD1]**	L2
		E strand	K 373 [NZ] K 373 [NZ] K 373 [NZ]	2.85 2.98 3.56	S 52 [OG] T 53 [OG1] **D 50 [O]**	L2 L2 L2	**D 362 [OD2]**	**3.69**	**R 54 [NH1]**	L2	**D 362 [OD2]**	**3.69**	**R 54 [NH1]**	L2
	L3	b-strand	**S 70 [O]** **S 72 [O]** Q 77 [NE2]	3.14 3.12 3.34	W 94 [NE1] N 93 [ND2] Y 92 [OH]	L3 L3 L3	**T 70 [O]** **S 72 [O]** Q 77 [NE2]	2.76 3.48 3.46	W 94 [NE1] N 93 [ND2] Y 92 [OH]	L3 L3 L3	**T 70 [O]** **S 72 [O]** Q 77 [NE2]	2.76 3.48 3.46	W 94 [NE1] N 93 [ND2] Y 92 [OH]	L3 L3 L3
		Fusion loop	R 99 [NH2] R 99 [NH1] R 99 [NH2] **G 104 [O]**	3.65 2.87 3.02 2.74	**N 93 [O]** N 93 [OD1] N 93 [OD1] **N 93 [N]**	L3 L3 L3 L3	R 99 [NH1] R 99 [NH2] **G 104 [O]**	3.1 2.98 2.86	N 93 [OD1] N 93 [OD1] **N 93 [N]**	L3 L3 L3	R 99 [NH1] R 99 [NH2] **G 104 [O]**	3.1 2.98 2.86	N 93 [OD1] N 93 [OD1] **N 93 [N]**	L3 L3 L3
Heavy chain	H1	*kl* loop					**S274 [N]**	3.3	E53 [OE2]	H1	**S274 [N]**	3.3	E53 [OE2]	H1
	H2	b-strand	**M 68 [O]** **M 68 [O]** **S 70 [N]** S 70 [OG]	3.72 3.22 3.14 2.94	S 56 [OG] **A 57 [N]** S 56 [OG] S 56 [OG]	H2 H2 H2 H2	**T 68 [O]** **T 70 [N]** T 70 [OG1] **E 84 [OE1]** **E 84 [OE2]**	3.11 3.23 2.96 **3.67** **3.71**	**A 57 [N]** S 56 [OG] S 56 [OG] **K 64 [NZ]** **K 64 [NZ]**	H2 H2 H2 H2 H2	**T 68 [O]** **T 70 [N]** T 70 [OG1] **E 84 [OE1]** **E 84 [OE2]**	3.11 3.23 2.96 **3.67** **3.71**	**A 57 [N]** S 56 [OG] S 56 [OG] **K 64 [NZ]** **K 64 [NZ]**	H2 H2 H2 H2 H2
		ij-loop	**R 252 [NH2]**	**3.37**	**D 55 [OD2]**	H2	**K 247 [NZ]** **K 247 [NZ]**	**3.84** **2.75**	**E 53 [OE1]** **D 55 [OD2]**	H2 H2	**K 247 [NZ]** **K 247 [NZ]**	**3.84** **2.75**	**E 53 [OE1]** **D 55 [OD2]**	H2 H2
		N67 glycan	no glycan at this position				**N67-1[O3]** **N67-1[O3]**	3.0 3.0	**G 65[O]** **G 65[O]**	H2 H2	**N67-1[O3]** **N67-1[O3]**	3.0 3.0	**G 65[O]** **G 65[O]**	H2 H2
	FH3	b-strand	**D 83 [OD1]**	**3.56**	**K 64 [NZ]**	FH3								
		N67 glycan	no glycan at this position				**N67-4[O2]** **N67-4[O2]**	2.70 3.32	S 82B[OG] S 82B[OG]	FH3 FH3	**N67-4[O2]** **N67-4[O2]**	2.70 3.32	S 82B[OG] S 82B[OG]	FH3 FH3
	H3	*ij*-loop	**Q 253 [N]** **Q 253 [O]**	3.11 3.37	Y 100 [OH] Y 100 [OH]	H3 H3	**Q 248 [N]**	3.03	Y 100 [OH]	H3	**Q 248 [N]**	3.03	Y 100 [OH]	H3

In bold red: main chain atoms involved in contacts; In bold black: salt bridges
Hydrogen bonds distances cut-off: 3.5Å; Salt bridges distances cut-off: ≤ 4Å